

RESEARCH ARTICLE

A metazoan-specific C-terminal motif in EXC-4 and $G\alpha$ -Rho/Rac signaling regulate cell outgrowth during tubulogenesis in *C. elegans*

Anthony F. Arena^{1,2,*}, Julianna Escudero^{1,†} and Daniel D. Shaye^{1,3,§}

ABSTRACT

Chloride intracellular channels (CLICs) are conserved proteins for which the cellular and molecular functions remain mysterious. An important insight into CLIC function came from the discovery that *Caenorhabditis elegans* EXC-4/CLIC regulates morphogenesis of the excretory canal (ExCa) cell, a single-cell tube. Subsequent work showed that mammalian CLICs regulate vascular development and angiogenesis, and human CLIC1 can rescue *exc-4* mutants, suggesting conserved function in biological tube formation (tubulogenesis) and maintenance. However, the cell behaviors and signaling pathways regulated by EXC-4/CLICs during tubulogenesis *in vivo* remain largely unknown. We report a new *exc-4* mutation, affecting a C-terminal residue conserved in virtually all metazoan CLICs, that reveals a specific role for EXC-4 in ExCa outgrowth. Cell culture studies suggest a function for CLICs in heterotrimeric G protein ($G\alpha/\beta/\gamma$)-Rho/Rac signaling, and Rho-family GTPases are common regulators of cell outgrowth. Using our new *exc-4* mutant, we describe a previously unknown function for $G\alpha$ -encoding genes (*gpa-12/G $\alpha_{12/13}$* , *gpa-7/G α_i* , *egl-30/G α_q* and *gsa-1/G α_s*), *ced-10/Rac* and *mig-2/RhoG* in EXC-4-mediated ExCa outgrowth. Our results demonstrate that EXC-4/CLICs are primordial players in $G\alpha$ -Rho/Rac-signaling, a pathway that is crucial for tubulogenesis in *C. elegans* and in vascular development.

KEY WORDS: EXC-4/CLIC, Rho/Rac, $G\alpha$, Outgrowth, Tubulogenesis

INTRODUCTION

Biological tubes are essential for the development and viability of multicellular organisms. For example, the cardiovascular circulatory system, composed of endothelial tubes required for nutrient and gas exchange, is the first organ system that forms during vertebrate development. The vasculature initially consists of wide-bore multicellular vessels, formed via a process termed ‘vasculogenesis’. These vessels later sprout and expand in response to developmental and environmental signals, via ‘angiogenesis’,

giving rise to tubes of different shapes and sizes, including thin, unicellular capillaries (reviewed by Xu and Cleaver, 2011; Iruela-Arispe and Beitel, 2013). Angiogenesis requires precise regulation of cell behaviors such as migration, growth, adhesion and fusion (Betz et al., 2016), and conserved aspects of how these behaviors are regulated at the genetic, molecular and cellular levels have been revealed by studies of models such as the *Caenorhabditis elegans* excretory system, which consists of three unicellular tubes (Fig. 1A; reviewed by Sundaram and Buechner, 2016; Shaye and Soto, 2021). We focus on one of these tubes: the excretory canal (ExCa) cell, which forms via ‘hollowing’ and cell outgrowth – a mechanism that is also deployed in angiogenesis (Kamei et al., 2006; Yu et al., 2015; Gebala et al., 2016). Many conserved regulators of ExCa tubulogenesis have been implicated in vascular development and disease (Choe and Strange, 2007; Tung et al., 2009; Ulmasov et al., 2009; Xie et al., 2009, 2013; Tung and Kitajewski, 2010; Dbouk et al., 2014; Lai et al., 2014; Lant et al., 2015; Tavasoli et al., 2016a; Mao et al., 2021). In addition, ExCa and neuronal outgrowth share common cellular and molecular features (reviewed by Sundaram and Buechner, 2016; Shaye and Soto, 2021), and regulators of neuronal outgrowth have also been implicated in vascular outgrowth and patterning (Adams and Eichmann, 2010). Therefore, studies of ExCa tubulogenesis provide insight into shared genetic and mechanistic aspects of vascular development and neuronal morphogenesis.

Here, we focus on the gene *exc-4*, which encodes a chloride intracellular channel (CLIC) required for ExCa outgrowth and lumen diameter maintenance (Fig. 1B,C; Buechner et al., 1999; Berry et al., 2003). A conserved role for CLICs in tubulogenesis was suggested by findings that mammalian CLIC1, CLIC4 and CLIC5 are expressed in the endothelium (Bohman et al., 2005; Tung et al., 2009; Ulmasov et al., 2009; Tung and Kitajewski, 2010; Tavasoli et al., 2016a), and that CLIC1 and CLIC4 regulate tubulogenesis of cultured primary human endothelial cells (Tung et al., 2009; Tung and Kitajewski, 2010). The mechanism by which CLICs regulate tubulogenesis are unknown, and physiologically relevant CLIC functions remain elusive (reviewed by Argenzio and Moolenaar, 2016). Indeed, despite their name, CLIC chloride channel activity under physiological conditions has not been demonstrated. CLICs also structurally resemble the omega family of glutathione-S-transferases (Ω -GSTs), and some CLICs have GST activity *in vitro*. However, the physiological relevance of this activity also remains unknown, and EXC-4/CLICs lacks the N-terminal cysteine critical for GST activity (Fig. 2A, arrowhead). Therefore, the tubulogenesis-regulating function of EXC-4/CLIC does not rely on GST-like activity.

CLICs have been linked to many cell behaviors, including migration, survival, differentiation, cytoskeletal regulation, and intracellular trafficking (reviewed by Argenzio and Moolenaar, 2016). Consistent with the numerous roles ascribed to CLICs, these

¹Department of Physiology and Biophysics, University of Illinois at Chicago - College of Medicine, Chicago, IL 60612, USA. ²Graduate Education in Biomedical Sciences program, University of Illinois at Chicago - College of Medicine, Chicago, IL 60612, USA. ³Center for Cardiovascular Research, University of Illinois at Chicago - College of Medicine, Chicago, IL 60612, USA.

*Present address: Evozyne, Chicago, IL 60614, USA. †Present address: Roy and Diana Vagelos Division of Biology and Biomedical Sciences, Washington University, St Louis, MO 63110, USA.

§Author for correspondence (shaye@uic.edu)

DOI: J.E., 0000-0002-7613-7332; D.D.S., 0000-0002-3962-6903

Handling Editor: Swathi Arur

Received 11 March 2022; Accepted 7 November 2022

proteins are found at various cellular locations and can re-localize in response to physiological and/or extracellular signals (reviewed by Argenzio and Moolenaar, 2016; see also Liang et al., 2017). EXC-4 constitutively localizes to the apical (lumen-lining) plasma membrane of the ExCa (Fig. 1D) via an N-terminal putative transmembrane domain (PTMD; Fig. 2A), and this localization is crucial for function (Berry et al., 2003; Berry and Hobert, 2006). The membrane-localized and tubulogenesis-regulating function of CLICs is conserved, because human CLIC1 can rescue *exc-4* mutants, but only when it is targeted to the ExCa apical membrane (Berry and Hobert, 2006).

A possible function for CLICs at the plasma membrane was suggested by findings that distinct G protein-coupled receptor (GPCR)-heterotrimeric G protein ($G\alpha/\beta/\gamma$)-Rho/Rac pathways promote rapid and transient CLIC re-localization from the cytoplasm to the plasma membrane in cultured cells (Ponsioen et al., 2009; Lecat et al., 2015). Given that key aspects of GPCR- $G\alpha/\beta/\gamma$ -Rho/Rac signaling occur at the plasma membrane (Syrovatkina et al., 2016; Mosaddeghzadeh and Ahmadian, 2021), these findings raised the possibility that CLICs could be new players in this pathway. Indeed, recent work shows that CLICs are required for GPCR-induced RhoA and/or Rac1 activation in cultured mammalian cells (Tavasoli et al., 2016b; Mao et al., 2021), and that CLIC1 and CLIC4 are required for RHOA- and RAC1-mediated angiogenic cell behaviors of primary human endothelial cells (Mao et al., 2021).

Many questions remain regarding the emerging function for CLICs in GPCR- $G\alpha/\beta/\gamma$ -Rho/Rac signaling. For example, it is not clear which, if any, of the proposed CLIC-regulated cellular behaviors are indeed mediated by CLIC-mediated GPCR- $G\alpha/\beta/\gamma$ -Rho/Rac signaling. It is also unknown whether the long-postulated channel or GST activities play a role in signaling, or whether CLIC-mediated signaling is limited to mammalian cells, or if this is a conserved and physiologically relevant CLIC function during development and/or disease. Here, using a new loss-of-function *exc-4* mutant, we show that EXC-4 regulates cell outgrowth via a highly conserved cysteine residue at the C terminus, which we found defines a new site that is not implicated in putative ion channel or GST activities of CLICs. In addition, genetic interaction between the new *exc-4* mutant and mutations in $G\alpha$ and Rho/Rac-encoding genes allowed us to define a heretofore-unknown role for $G\alpha$ and Rho/Rac signaling in ExCa outgrowth, and to demonstrate that *exc-4* functions within this pathway in ExCa tubulogenesis. Our work not only defines a previously unappreciated role for EXC-4/CLICs in cell outgrowth *in vivo*, it also suggests that CLIC proteins are ancient players in $G\alpha$ -Rho/Rac signaling.

RESULTS

An *exc-4* loss-of-function mutation in a highly conserved C-terminal site affects ExCa outgrowth

All previously described *exc-4* alleles are nulls, hereafter (0), causing strong and fully penetrant cystic and shortened ExCa defects (Fig. 1B,C; Buechner et al., 1999; Berry et al., 2003). As ExCa cysts in *exc-4(0)* animals are large (Fig. 1C,E), it was not possible to determine whether the outgrowth defect is secondary to the lumen maintenance phenotype, or whether *exc-4* has separable functions that regulate these two cellular processes. It is also difficult to use *exc-4(0)* mutations to evaluate genetic interactions, as their strength and penetrance makes it challenging to assess whether mutations in other genes can exacerbate ExCa phenotypes. Moreover, mutations in other genes that might modify (suppress or enhance) phenotypes caused by *exc-4* loss may not be apparent if

EXC-4 protein is wholly absent or non-functional. To circumvent these challenges, we sought to identify hypomorphic, or reduced function, *exc-4* alleles (see Materials and Methods) and found a mutation changing a highly conserved C-terminal Cys (Fig. 2A; EXC-4 Cys237) to Tyr that affects ExCa outgrowth (see Fig. 1B for outgrowth scoring criteria) and behaves like an *exc-4* hypomorph (Fig. 1B,C). We refer to this mutation as *exc-4(rf)* hereafter.

Because apical membrane localization is essential for EXC-4 function (Berry et al., 2003; Berry and Hobert, 2006), we investigated whether EXC-4 Cys237 promotes apical localization. We created constructs carrying the ExCa promoter *glt-3p* (Shaye and Greenwald, 2015) followed by the yellow fluorescent protein Venus, an EXC-4::Venus fusion, or mutant EXC-4^{C237Y}::Venus, generated transgenes carrying these constructs (see Materials and Methods), and we crossed these transgenes into *exc-4(0)* mutants to assess Venus accumulation in the absence of endogenous EXC-4, as it is possible that wild-type protein could compensate for any localization defects caused by the C237Y mutation. We found that EXC-4^{C237Y}::Venus, like wild-type protein, localized to the apical membrane (Fig. 1D), and thus conclude that Cys237 is not required for EXC-4 localization.

We note that *exc-4(rf)* mutants did not display the cystic phenotype seen in *exc-4(0)*, although small swellings were often visible at the end of shortened posterior canals in these mutants (Fig. 1B, Fig. S1). Small swellings, also called ‘varicosities’ or ‘pearls’, could be seen in early stages of ExCa tubulogenesis (Fig. S1A) and are postulated to represent areas of active lumen growth that ‘resolve’ upon ExCa outgrowth (reviewed by Sundaram and Buechner, 2016; Shaye and Soto, 2021). In contrast, ExCa cysts, which we previously defined as lumen expansions encompassing at least a quarter of body width (Shaye and Greenwald, 2015, 2016; see Fig. 1B for cyst scoring criteria) are found in mutants affecting apical vesicle trafficking, exocytosis, or the lumen-lining apical cytoskeleton – mechanisms that regulate ExCa lumen diameter and coordinate lumen and basolateral cell outgrowth (reviewed by Sundaram and Buechner, 2016; Shaye and Soto, 2021). Our finding that *exc-4(rf)* mutants do not have a significant cystic phenotype led us to hypothesize that EXC-4 has separable lumen maintenance and outgrowth functions, and that EXC-4 Cys237 is more important for the latter. If this were the case, then we would expect that re-introducing wild-type EXC-4 into *exc-4(0)* mutants should rescue both phenotypes, whereas transgenes expressing EXC-4^{C237Y} should preferentially, or only, rescue the cystic phenotype. To test this hypothesis, we generated multi-copy transgenes expressing EXC-4::Venus (*arIs190*) or EXC-4^{C237Y}::Venus (*vasIs2*) that were randomly integrated into the genome to reduce expression heterogeneity between individuals (see Materials and Methods). We found that these multi-copy transgenes rescued both the outgrowth and cystic defects of *exc-4(0)* mutants; however, the transgene expressing EXC-4::Venus was significantly better at rescuing than the EXC-4^{C237Y}::Venus transgene (Fig. S1D,E), consistent with our hypothesis. The partial rescue seen with EXC-4^{C237Y}::Venus might indicate that Cys237 is not absolutely required for ExCa outgrowth. Alternatively, residual rescue may be due to overexpression of the hypomorphic EXC-4^{C237Y} protein. To address this possibility, and to avoid the effects of unregulated overexpression inherent with multi-copy arrays (Nance and Frøkjær-Jensen, 2019), we repeated this experiment using Mos1-mediated single-copy insertion (MosSCI; see Frøkjær-Jensen, 2015) to create single-copy transgenes, integrated into a unique genomic locus, expressing EXC-4 or EXC-4^{C237Y} (see Materials and Methods). The EXC-4-expressing transgene (*vasSi11*) significantly rescued both the outgrowth and the cystic phenotypes of *exc-4(0)*

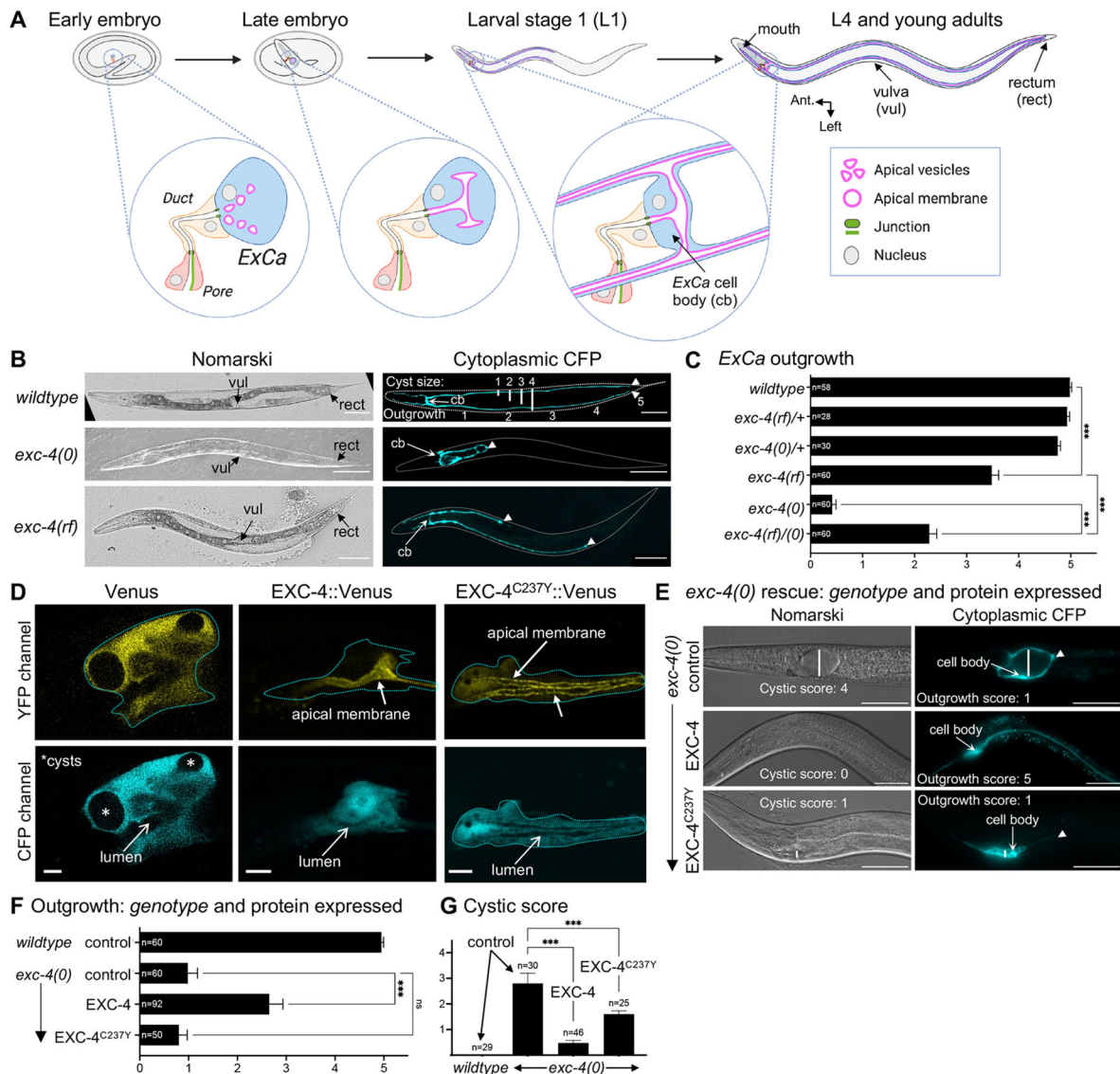


Fig. 1. ExCa tubulogenesis and a new hypomorphic *exc-4* mutation. (A) Summary of excretory system development (reviewed by Sundaram and Buechner, 2016; Shaye and Soto, 2021). The pore (red), duct (yellow) and excretory canal (ExCa) cell (blue) form tubes during embryogenesis that remain interconnected via ring-shaped adherens junctions (AJs; green). In the early embryo, intracellular vesicles in the ExCa traffic towards the AJ where they fuse to form the nascent lumen. A microtubule-, F-actin- and intermediate filament-rich cytoskeleton forms at the apical membrane (magenta), which limits lumen diameter and promotes fluid-mediated extension. In late embryos, the growing ExCa lumen bifurcates into left and right canals and these later split into anterior and posterior canals. The apical lumen and basolateral membrane (dark blue line) grow from the ExCa cell body (cb) in a coordinated manner, a process we term 'outgrowth'. Posterior canals have only grown to approximately half length when animals hatch into L1 larvae, and outgrowth is completed before they molt into L2. An L4 hermaphrodite highlighting morphological features, the vulva (vul) and rectum (rect), which we used to score ExCa outgrowth (see Materials and Methods). (B) Nomarski interference contrast and wide-field fluorescence microscopy images of control (wild type; *arl159*), *exc-4(rh133)* [hereafter (0)] and *exc-4(gk451333)* [hereafter *exc-4(rf)*], hermaphrodites expressing cytoplasmic CFP (cyan) in the ExCa. Cystic and outgrowth scoring criteria are shown in the 'Cytoplasmic CFP' control panel. Posterior ExCa tips (arrowheads here and in subsequent micro-photographs) reach the rectum in controls, whereas in *exc-4(0)* mutants the ExCa forms large cysts and little outgrowth is seen. In *exc-4(rf)* mutants, ExCa outgrowth is compromised, but cysts are not formed. Scale bars: 100 µm. (C) Quantification of posterior ExCa outgrowth (see Materials and Methods). Bars denote the mean outgrowth score for each genotype and error bars represent the 95% confidence interval. Significance was calculated by one-way ANOVA with Bonferroni correction for multiple comparisons; ***P<0.0001. A bona fide hypomorphic *exc-4* mutation should fit the following three criteria: (1) cause ExCa defects similar to, but milder than, those seen in *exc-4(0)* mutants; (2) be recessive; and (3) fail to complement *exc-4(0)*. The new *exc-4(rf)* allele displays these three properties. (D) Confocal images of the ExCa cell body, marked with cytoplasmic CFP, in *exc-4(0)* hermaphrodites with transgenes expressing either Venus alone (*vasSi1*), EXC-4::Venus (*vasEx1*) or EXC-4^{C237Y}::Venus (*vasIs2*). Venus alone is cytoplasmic and does not rescue *exc-4(0)*. Asterisks indicate cysts caused by *exc-4* loss. Wild-type EXC-4::Venus rescues *exc-4(0)* and localizes to the lumen-lining apical membrane. The bright disk in this image is the ExCa nucleus, with dark nucleolus in the middle. EXC-4^{C237Y}::Venus localizes to the apical membrane, but fails to rescue *exc-4(0)*, as evidenced by the continued presence of large cysts. Scale bars: 5 µm. (E) Representative Nomarski and CFP fluorescence images of *exc-4(0)* rescue. Control animals (expressing Venus from the single-copy insertion *vasSi1*) display strong outgrowth and cystic defects (quantified in F,G). A single-copy insertion expressing wild-type EXC-4 in the ExCa (*vasSi11*) significantly rescues both *exc-4(0)* phenotypes, whereas a single-copy insertion at the same genomic location (*vasSi16*; see Materials and Methods) expressing EXC-4^{C237Y} fails to rescue the *exc-4(0)* outgrowth defect but significantly rescues the cystic phenotype (see also Fig. S1D,E). Scale bars: 50 µm. (F,G) Rescue of *exc-4(0)* outgrowth (F) and cystic (G) defects by EXC-4- and EXC-4^{C237Y}-expressing single-copy insertions. One-way ANOVA, with Bonferroni correction for multiple comparisons, was used to calculate significance; ***P<0.001. ns, not significant.

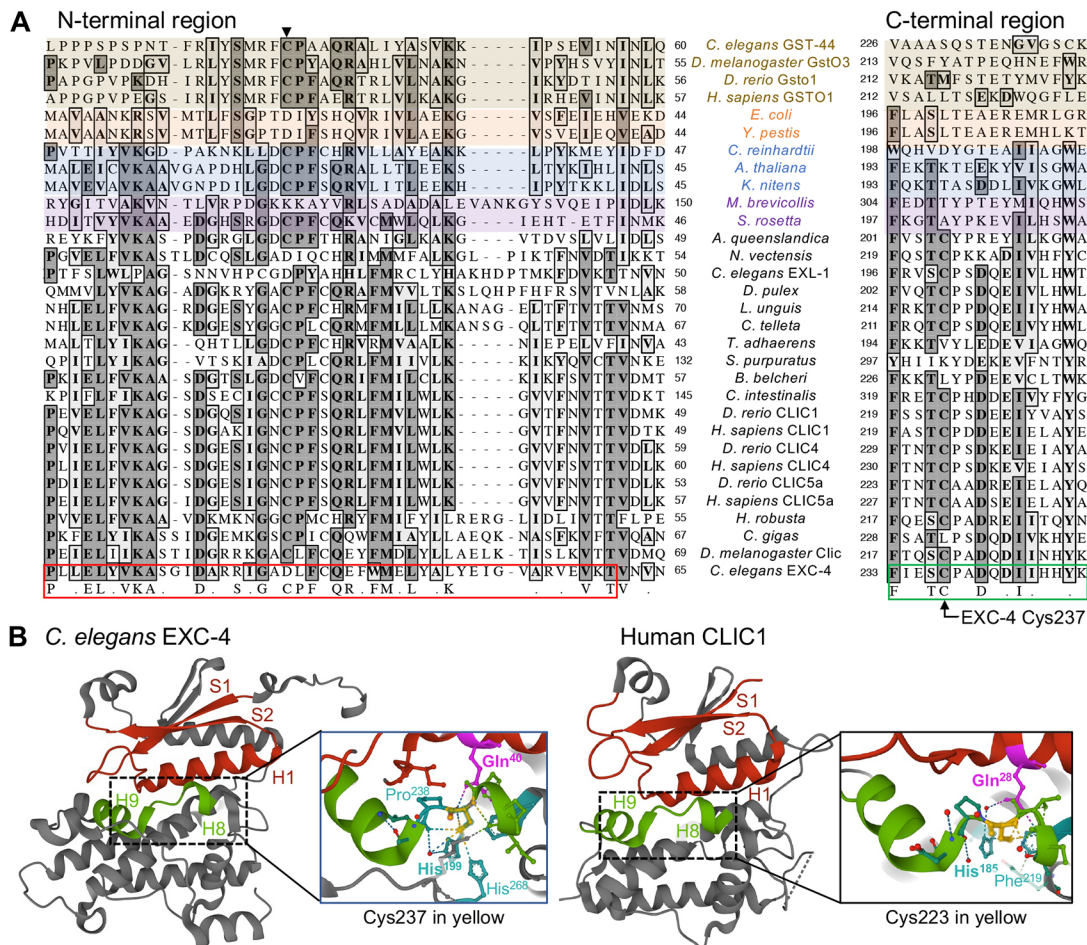


Fig. 2. Alignment of GST-Ω and CLICs, and structural comparison of the conserved C-terminal Cys in *C. elegans* EXC-4 and human CLIC1.

(A) CLUSTALW alignment (see Materials and Methods) of the N-terminal and C-terminal regions of: GST-Ω proteins from *C. elegans*, *Drosophila*, zebrafish and human (brown), CLIC proteins from bacteria (orange), plants and algae (blue), choanoflagellate (purple) and metazoa (black). Full-length protein alignments are shown in Fig. S2. An N-terminal cysteine required for thiol-transferase activity (arrowhead) is not conserved in EXC-4. The EXC-4 and consensus N-terminal PTMD (Berry and Hobert, 2006; Littler et al., 2008) are highlighted by a red box. The cysteine mutated in *exc-4(rf)*, EXC-4^{C237} and surrounding conserved C-terminal motif are highlighted by the green box. (B) Crystal structures of *C. elegans* EXC-4 (PDB ID# 2YV9; Littler et al., 2008) and human CLIC1 (PDB ID# 1K00; Harrop et al., 2001) were obtained from the RCSB PDB database (Berman et al., 2000; Burley et al., 2021) and visualized using the Mol* viewer (Sehnal et al., 2021). CLICs consist of two discrete domains: the N-terminal domain composed of four β-sheets interspersed between three α-helices, and the C-terminal domain composed of six or seven α-helices (Harrop et al., 2001; Littler et al., 2008). The PTMD, consisting of two β-sheets (S1, S2) flanking the first α-helix (H1), is highlighted in red. The conserved C-terminal motif (green) encompasses H8 and H9, with the conserved Cys found in the loop between these helices. The conserved Cys (yellow) interacts with a conserved Gln in H1 (magenta), and makes extensive contacts with residues in H6, H8 and H9 (teal), as described in the text.

(Fig. 1E-G), although rescue was less robust than that seen with the multi-copy transgene *arls190* (Fig. S1D,E), consistent with lower expression levels from the single-copy insertion. In contrast, the EXC-4^{C237Y} single-copy transgene (*vasSi16*) rescued the cystic phenotype, but not the outgrowth defect of *exc-4(0)* (Fig. 1E-G), supporting our model that EXC-4 lumen maintenance and cell outgrowth functions are separable and that EXC-4^{C237} is mainly required for the latter.

EXC-4^{C237} defines a conserved C-terminal motif found only in metazoan CLICs

If the activity imparted by EXC-4^{C237} is important for a conserved function, then we expect that this residue, and nearby sequences, would be conserved in evolutionarily distant CLICs. To expand our analysis beyond the previously described bacterial, plant and bilaterian (*C. elegans*, *Drosophila* and mammalian) CLICs we performed BLASTP searches (see Materials and Methods),

and identified putative CLICs from two algae (*Klebsormidium nitens* and *Chlamydomonas reinhardtii*), two choanoflagellates (*Monosiga brevicollis* and *Salpingoeca rosetta*), which are the closest unicellular relatives to metazoans (Ros-Rocher et al., 2021), and from 11 additional bilaterian species. We also identified CLIC orthologs in representative species from three out of the four ‘basal’ metazoan clades that emerged, along with bilateria, from a last common ancestor of all metazoans (Littlewood, 2017; Li et al., 2021; Ros-Rocher et al., 2021). The three CLIC orthologs from non-bilaterian metazoans are from the sponge (porifera) *Amphimedon queenslandica*, the placozoan *Trichoplax adhaerens* and the sea anemone (cnidarian) *Nematostella vectensis*. Notably, we did not identify a CLIC in any of the five sequenced comb jelly (ctenophora) species representing the fourth basal metazoan clade. This was surprising given the existence of putative CLIC orthologs in prokaryotes and plants (Elter et al., 2007; Gururaja Rao et al., 2017), and our finding of CLICs in algae and choanoflagellates.

These observations suggests that an ancestral CLIC-like protein (present in prokaryotes, algae, plants and choanoflagellates) was lost from ctenophores, which is consistent with the hypothesis that ctenophores are the most diverged metazoan branch (Li et al., 2021).

We aligned GST- Ω and CLIC proteins (see Materials and Methods and Fig. S2) and focused on the N-terminal PTMD region (Fig. 2A, red box) and the C-terminal region where EXC-4^{C237} resides (Fig. 2A, green box), as these two sites are required for EXC-4 function in the ExCa. At the N terminus, we found that CLICs have a highly conserved ~40 amino-acid stretch, beginning with consensus EL[F/W/Y]VKA[A/S/G] and ending with VxTV (Fig. 2A, red). This region encompasses two β -sheets (S1 and S2) flanking an α -helix (H1) in EXC-4 and CLIC1 (Fig. 2B, red) that make up the conserved EXC-4/CLIC PTMD (Berry and Hobert, 2006; Littler et al., 2008). We note that an N-terminal Cys residue (Fig. 2A, arrowhead) required for GST- Ω catalytic activity (Board et al., 2000) is absent from several CLICs, including EXC-4, suggesting that the canonical thioltransferase activity of GST- Ω is not strictly required for an evolutionarily conserved EXC-4/CLIC function.

We also found that the C terminus of metazoan CLICs have a highly conserved motif, consensus Fxx[S/T]CxxDx[D/E]Ixxx[W/Y], flanking the residue mutated in *exc-4(rf)*: EXC-4^{C237} (Fig. 2A, green box). In addition to sequence conservation, this Cys is predicted to have conserved interactions (Fig. 2B) with a glutamine residue in H1 (Gln⁴⁰ in EXC-4, Gln²⁸ in human CLIC1) and a histidine in H6 (His¹⁹⁹ in EXC-4, His¹⁸⁵ in CLIC1; Fig. 2B, blue). The conserved Cys also makes contacts with other residues within the C-terminal motif (e.g. with Pro²³⁸ in EXC-4, with Phe²¹⁹ in CLIC1; Fig. 2B, blue), perhaps lending stability to this motif. Moreover, the conserved Gln in H1 also interacts with the Ser/Thr residue directly upstream of the conserved Cys (Ser²³³ in EXC-4, Thr²²² in CLIC1; not shown). These observations suggest that the C-terminal motif defined by EXC-4^{C237Y} promotes a conserved EXC-4/CLIC structure and is thus likely critical for a conserved function. We also note that the Cys-based motif is absent from GST- Ω proteins, suggesting that this residue is not associated with GST activity. In addition, the absence of the C-terminal Cys in bacterial and *Arabidopsis* CLICs, both of which have ion channel function (Elter et al., 2007; Gururaja Rao et al., 2017), suggests that this motif is not associated with CLIC channel activity.

To examine the evolutionary history of CLICs, with a focus on defining the emergence of the C-terminal cysteine-based motif described here, we generated a phylogenetic tree of GST- Ω and CLIC proteins (see Materials and Methods and Fig. S3). All the eukaryotic CLICs grouped together, whereas bacterial CLICs clustered with GST- Ω s, suggesting that these proteins may be more closely related to GSTs. Most metazoan CLICs clustered together, the exception being that from the sponge *A. queenslandica*, which grouped with *Arabidopsis*, algal and choanoflagellate proteins. This is consistent with the well-known divergence between sponges and other metazoans (Littlewood, 2017; Li et al., 2021). CLIC-like proteins from *Arabidopsis*, *K. nitens* and the two choanoflagellate species have a degenerate C-terminal motif, lacking a cysteine, whereas an intact motif is present in CLICs from *A. queenslandica*, *N. vectensis*, and in 14/17 (~82%) of the bilaterian CLICs examined (Fig. 2A). These observations suggest that the cysteine corresponding to EXC-4^{C237} arose with the emergence of metazoans, and, although this residue has been sporadically lost (e.g. in CLICs from the placozoan *T. adhaerens*, echinoderms, cephalochordates and mollusks; see Materials and Methods and Fig. S3), the continued presence of this

Cys-based motif suggests that EXC-4^{C237} mediates an ancient function that arose in metazoan CLICs.

Genetic interactions reveal a role for G α orthologs in EXC-4-mediated ExCa outgrowth

Because CLICs have been implicated in GPCR-G α / β / γ -Rho/Rac signaling in cell culture, and Rho/Rac GTPases regulate cell outgrowth, a function that has been extensively studied in *C. elegans* neurons (Zipkin et al., 1997; Lundquist et al., 2001; Nørgaard et al., 2018), we next investigated whether functional interactions between EXC-4 and a GPCR-G α / β / γ -Rho/Rac pathway influence ExCa outgrowth. There are ~1500 GPCR-encoding genes in *C. elegans* (Fredriksson et al., 2003; Vidal et al., 2018), and, due to this expansion, as well as extensive sequence divergence, it is challenging to define specific *C. elegans* orthologs of vertebrate GPCRs (Shaye and Greenwald, 2011; Kim et al., 2018). Consequently, there are no obvious orthologs of the GPCRs linked to CLIC regulation and function in mammalian cells (Ponsioen et al., 2009; Lecat et al., 2015; Argenzio et al., 2018; Mao et al., 2021). Therefore, we instead focused on assessing the function of G α , Rho and Rac orthologs in EXC-4-mediated ExCa outgrowth.

Eight *C. elegans* G α -encoding genes have clear mammalian orthologs (Jansen et al., 1999; Bastiani and Mendel, 2006; Shaye and Greenwald, 2011; Kim et al., 2018): four are G α_i -encoding genes (*gpa-4*, *gpa-7*, *gpa-16* and *odr-3*), and the remaining are G $\alpha_{12/13}$, G α_o , G α_q and G α_s orthologs (*gpa-12*, *goa-1*, *egl-30* and *gsa-1*, respectively). Predicted null mutants of most G α -encoding genes, except *gpa-16*/G α_i , *egl-30*/G α_q and *gsa-1*/G α_s , are viable (Brundage et al., 1996; Korswagen et al., 1997; Jansen et al., 1999; Bergmann et al., 2003). We examined the ExCa in these viable G α mutants, as well as in animals with strong loss-of-function or activating mutations in essential G α_s , and did not observe ExCa phenotypes in any of these single mutants (Fig. 3, Fig. S4). We next assessed genetic interactions between the *exc-4(rf)* allele and G α mutations and found that neither mutation of *goa-1*/G α_o , nor of three of the four G α_i orthologs, modified the *exc-4(rf)* phenotype (Fig. S4A). In contrast, *exc-4(rf)* genetically interacted with mutations in *egl-30*/G α_q , *gpa-12*/G $\alpha_{12/13}$, *gsa-1*/G α_s and *gpa-7*/G α_i (Fig. 3; discussed below), suggesting that these G α genes play a role in *exc-4*-mediated ExCa outgrowth.

The *exc-4(rf)* outgrowth defect was significantly suppressed by a hypomorphic *egl-30*/G α_q mutation (Brundage et al., 1996) and by a deletion of almost the entire *gpa-12*/G $\alpha_{12/13}$ genomic region (Hiley et al., 2006). In contrast, both an activated *gsa-1*/G α_s (Schade et al., 2005) and a *gpa-7*/G α_i deletion allele (Jansen et al., 1999) significantly exacerbated the *exc-4(rf)* outgrowth phenotype. Because activation of *gsa-1*/G α_s enhanced, whereas loss of *egl-30*/G α_q or *gpa-12*/G $\alpha_{12/13}$, suppressed, the *exc-4(rf)* outgrowth phenotype we hypothesized that these three G α proteins impinge on *exc-4* function in a similar manner, and examined whether they are functionally redundant by constructing double and triple loss-of-function mutant strains (see Materials and Methods). We also examined a double-mutant strain carrying *gsa-1(act)* and *egl-30(act)* alleles. However, none of these strains exhibited ExCa outgrowth defects (Fig. S4B), suggesting that other G α proteins, or perhaps other pathways, might functionally compensate for loss or activation of these G α proteins. Because the *exc-4* allele used to define interactions with G α -encoding genes is non-null, it is not possible to define precisely the functional relationship between EXC-4 and G α proteins based on these results. However, our results demonstrate, for the first time, that G α proteins play a role in

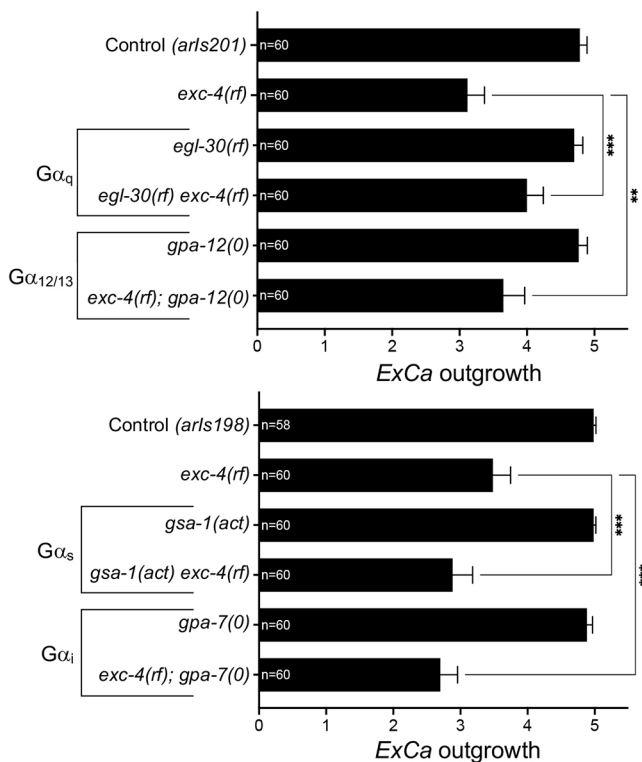


Fig. 3. *exc-4(rf)* genetically interacts with mutations in Gα-encoding genes. Top: An *egl-30*/Gα_q hypomorph, *egl-30(ad805)* (Brundage et al., 1996), and a *gpa-12*/Gα_{12/13} null, *gpa-12(pk322)* (Jansen et al., 1999; van der Linden et al., 2003), both suppress the *exc-4(rf)* outgrowth defect. Bottom: In contrast, *gsa-1(ce81)*, an activated *gsa-1*/Gα_s allele (Schade et al., 2005), and *gpa-7(pk610)*, a deletion of *gpa-7*/Gα_i (Jansen et al., 1999), both enhance *exc-4(rf)*. See Table S1 for full genotypes. Bars indicate average posterior ExCa outgrowth (see Materials and Methods) and error bars are the 95% confidence interval. One-way ANOVA with Bonferroni correction for multiple comparisons was used to calculate significance; ***P*<0.01; ****P*<0.001.

EXC-4-mediated cell outgrowth during tubulogenesis, and that a functional interaction between Gα-mediated signaling and EXC-4/CLIC proteins is evolutionarily conserved.

CED-10 and MIG-2 function in parallel in the ExCa to promote outgrowth

We next investigated a role for Rho and Rac orthologs in ExCa outgrowth. *C. elegans* has four genes encoding canonical Rho/Rac GTPases: *ced-10/Rac*, *mig-2/RhoG*, *rac-2/Rac* and *rho-1/RhoA* (Reiner and Lundquist, 2018). Previous work showed that *rho-1* does not play a major role in ExCa outgrowth (Marcus-Gueret et al., 2012); thus, we focused our analysis on the three other Rho/Rac-encoding genes. We analyzed several *ced-10* loss-of-function alleles: a genomic deletion, hereafter *ced-10(0)*, resulting in maternally rescued homozygous-sterile animals; a mutation in the C-terminal 'CAAX' box, which is required for CED-10 membrane localization; and mutations in the 'switch 1' or 'switch 2' regions, which interact with upstream regulators and/or downstream effectors (see Fig. 4A; Reddien and Horvitz, 2000; Lundquist et al., 2001; Zhuravlev et al., 2017; Nørgaard et al., 2018). These loss-of-function mutations all resulted in significant ExCa shortening (Fig. 4B), indicating that *ced-10* promotes ExCa outgrowth. A second Rac-encoding gene, *rac-2*, is redundant with *ced-10* in some (Lundquist et al., 2001; Struckhoff and Lundquist,

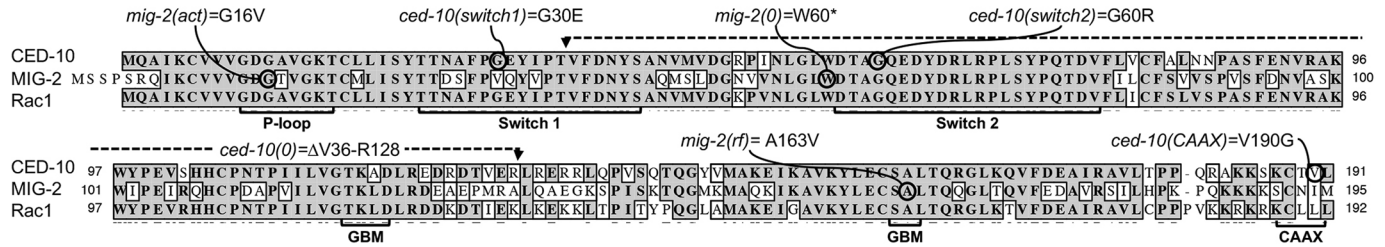
2003; Shakir et al., 2006), but not all (Peters et al., 2013; Nørgaard et al., 2018), contexts. We found that a *rac-2* deletion (see Materials and Methods) did not cause ExCa phenotypes on its own, nor did it exacerbate those caused by *ced-10* loss-of-function mutations (Fig. S5A). Thus, we conclude that *rac-2* does not function redundantly with *ced-10* in ExCa outgrowth. We also examined a CRISPR-generated activated *ced-10* allele, called *ced-10(knu268)*, based on the well-studied mutation of a conserved Pro residue in the 'switch 1' region (P29S in CED-10; Nørgaard et al., 2018). However, we found that *ced-10(knu268)* did not act in a dominant manner, as would be expected for an activating-mutation, and instead was indistinguishable from *ced-10(0)* mutants, both on its own or when combined with the *exc-4(rf)* mutation (see next section). Therefore, we did not examine this mutant further.

The gene *mig-2* encodes a protein with a sequence that is most similar to Rac1 but is functionally related to RhoG (deBakker et al., 2004; Reiner and Lundquist, 2018). We analyzed three *mig-2* alleles (Fig. 4A; Zipkin et al., 1997; Lundquist et al., 2001): a *mig-2(0)* resulting from an early nonsense mutation; a hypomorphic *mig-2(rf)* allele, resulting from a mutation affecting a guanine-binding motif, and a *mig-2(act)* allele, and these mutants all showed ExCa outgrowth defects (Fig. 4C). The fact that loss-of-function and activating *mig-2* mutations cause similar phenotypes has been reported in other contexts (Zipkin et al., 1997; Nørgaard et al., 2018), and it has been suggested that this may be due to the fact that proper Rho-family GTPase function requires cycling between 'on' and 'off' states (Zipkin et al., 1997). We note that genetic interactions between *exc-4(rf)* and *mig-2(act)* are distinct from those seen between *exc-4(rf)* and *mig-2* loss-of-function alleles (Fig. 5C), consistent with loss-of-function and activating mutations having distinct effects on *mig-2* activity even though they show similar phenotypes as single mutants.

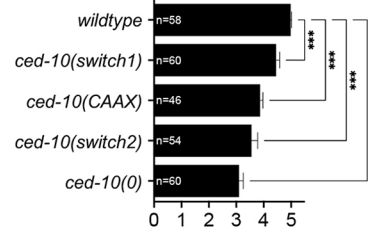
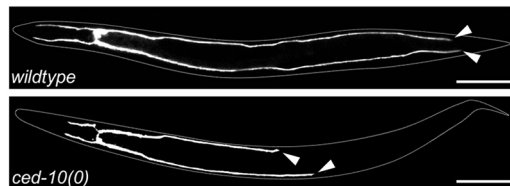
Because *ced-10/Rac* and *mig-2/RhoG* often function redundantly (Lundquist et al., 2001; Kishore and Sundaram, 2002; Struckhoff and Lundquist, 2003; Shakir et al., 2006, 2008; Nørgaard et al., 2018), we examined whether this was the case in ExCa outgrowth by building strains carrying combinations of *ced-10* and *mig-2* loss-of-function alleles, including double-null mutants, and we found a more severe defect in these doubles than in any individual single mutant (Fig. 4D), indicating that *ced-10* and *mig-2* act in parallel to promote ExCa outgrowth.

To define the cellular focus of CED-10 function in ExCa outgrowth, we made *vasEx34*, an extrachromosomal multi-copy array, and *vasTi2*, a single-copy genome-inserted transgene, both carrying the ExCa promoter *glt-3p* followed by sequences encoding FLAG-tagged CED-10 (see Materials and Methods), and both transgenes rescued *ced-10(0)* mutants (Fig. 4E), indicating that *ced-10* functions cell autonomously to promote ExCa outgrowth. Because the ExCa outgrowth defect of *mig-2(0)* single mutants is mild (Fig. 4C), we investigated the focus of MIG-2 function using the stronger *ced-10(0); mig-2(0)* double mutant background; an approach previously used to define the site of *mig-2* function in neuronal migration and outgrowth (Lundquist et al., 2001). We note that the extrachromosomal array *vasEx34* (described above) rescues *ced-10(0); mig-2(0)* double mutants (Fig. 4F), indicating that this approach is feasible in the ExCa. However, neither genome-inserted single-copy transgenes, nor multi-copy extrachromosomal transgenes, carrying *glt-3p::FLAG::MIG-2* rescued *ced-10(0); mig-2(0)* ExCa outgrowth defects (data not shown). In contrast, a multi-copy extrachromosomal transgene carrying *glt-3p*-driven untagged MIG-2 (*qvEx590*; kindly provided by R. Dima and C. Bénard,

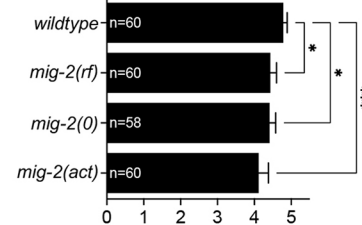
A CED-10/Rac and MIG-2/RhoG sequences and mutations



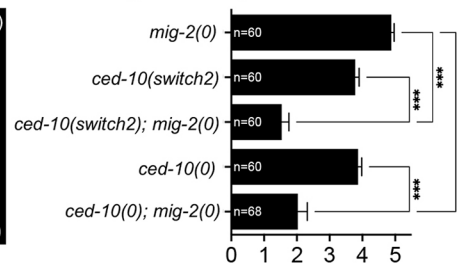
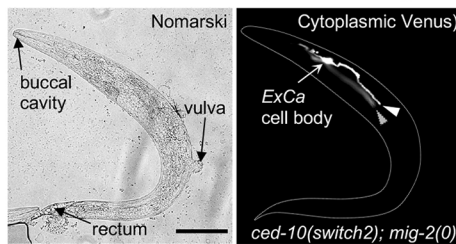
B ExCa outgrowth in *ced-10* mutants



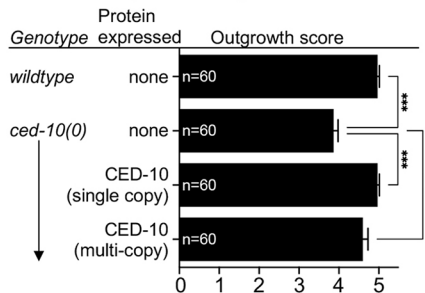
C ExCa outgrowth in *mig-2* mutants



D *ced-10*/Rac and *mig-2*/RhoG regulate ExCa outgrowth in parallel



E ExCa-specific expression of CED-10



F ExCa-specific expression of MIG-2

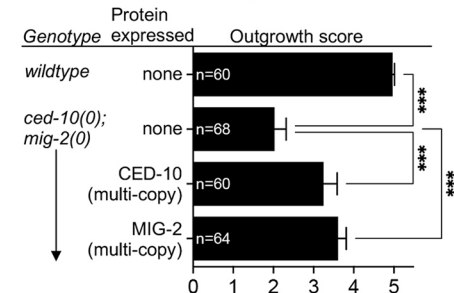


Fig. 4. *ced-10* and *mig-2* function in parallel in the ExCa to promote outgrowth. (A) Full-length sequence alignment of *C. elegans* CED-10, MIG-2 and human RAC1. Conserved domains (reviewed by Reiner and Lundquist, 2018), such as the phosphate binding P-loop, the effector-binding switch 1 and switch 2 regions, the guanine-binding motifs (GBM) and the C-terminal lipid-modified 'CAAX' sequence are highlighted by brackets. Amino-acid changes associated with different alleles are shown. (B) Left: Fluorescent micrographs showing cytoplasmic CFP in the ExCa of control and maternally rescued *ced-10* zygotic null (*0*) animals homozygous for the large deletion allele *ced-10(n3417)* (Lundquist et al., 2001). Arrowheads indicate the extent of posterior ExCa outgrowth. Scale bars: 100 μm. Right: Quantification of ExCa outgrowth in control animals and in animals homozygous for: *ced-10* loss-of-function mutations affecting the switch 1 region [*ced-10(rp100)*; Norgaard et al., 2018], the CAAX sequence or the switch 2 regions [*ced-10(n1993)* or *ced-10(n3246)*, respectively; see Reddien and Horvitz, 2000], and the *ced-10(0)* deletion. (C) ExCa outgrowth in control and in animals homozygous for: a *mig-2* mutation affecting the second GBM, leading to reduced function (*rf*), an early stop predicted to be a *mig-2(0)* mutant, and an activating (*act*) mutation [*mig-2(gm38)*, *mig-2(mu28)* and *mig-2(gm103)*, respectively; see Forrester and Garriga, 1997; Zipkin et al., 1997; Forrester et al., 1998]. (D) Left: Nomarski interference contrast image and corresponding fluorescence micrograph showing cytoplasmic CFP in the ExCa of a *ced-10(n3246); mig-2(mu28)* double mutant. Note the protruding vulva in the Nomarski image, indicating that this animal, although small, has reached adulthood. Arrowheads indicate the extent of posterior ExCa outgrowth. Scale bar: 100 μm. Right: Quantification of ExCa outgrowth in *ced-10* and *mig-2* single- or double-mutant strains. (E) *vasT12*, a single-copy genomic insertion transgene carrying *glt-3p::FLAG::ced-10*, and *vasEx34*, a multi-copy extrachromosomal array carrying *mScarlet(l)::3xFLAG::ced-10* (see Materials and Methods), both significantly rescue the ExCa outgrowth defect of *ced-10(0)* mutants. (F) *vasEx34* and *qvEx590*, a multi-copy extrachromosomal array (kindly provided by R. Dima and C. Bénard) carrying *glt-3p::mig-2*, both significantly rescue the severe outgrowth phenotype of *ced-10(0); mig-2(0)* double mutants. See Table S1 for full genotypes. In the graphs, solid bars denote average posterior ExCa outgrowth (see Materials and Methods) and error bars represent the 95% confidence interval. One-way ANOVA with Bonferroni correction for multiple comparisons was used to calculate significance; **P*<0.05; ****P*<0.001.

Université de Québec, Montréal, Canada) efficiently rescued the *ced-10(0); mig-2(0)* ExCa outgrowth defect (Fig. 4F). Therefore, we conclude that *mig-2* also functions cell-autonomously to

promote ExCa outgrowth, and that, unlike for CED-10, an N-terminal FLAG-tag appears to interfere with MIG-2 function. Our discovery of a cell-autonomous function for *ced-10* and *mig-2* in the

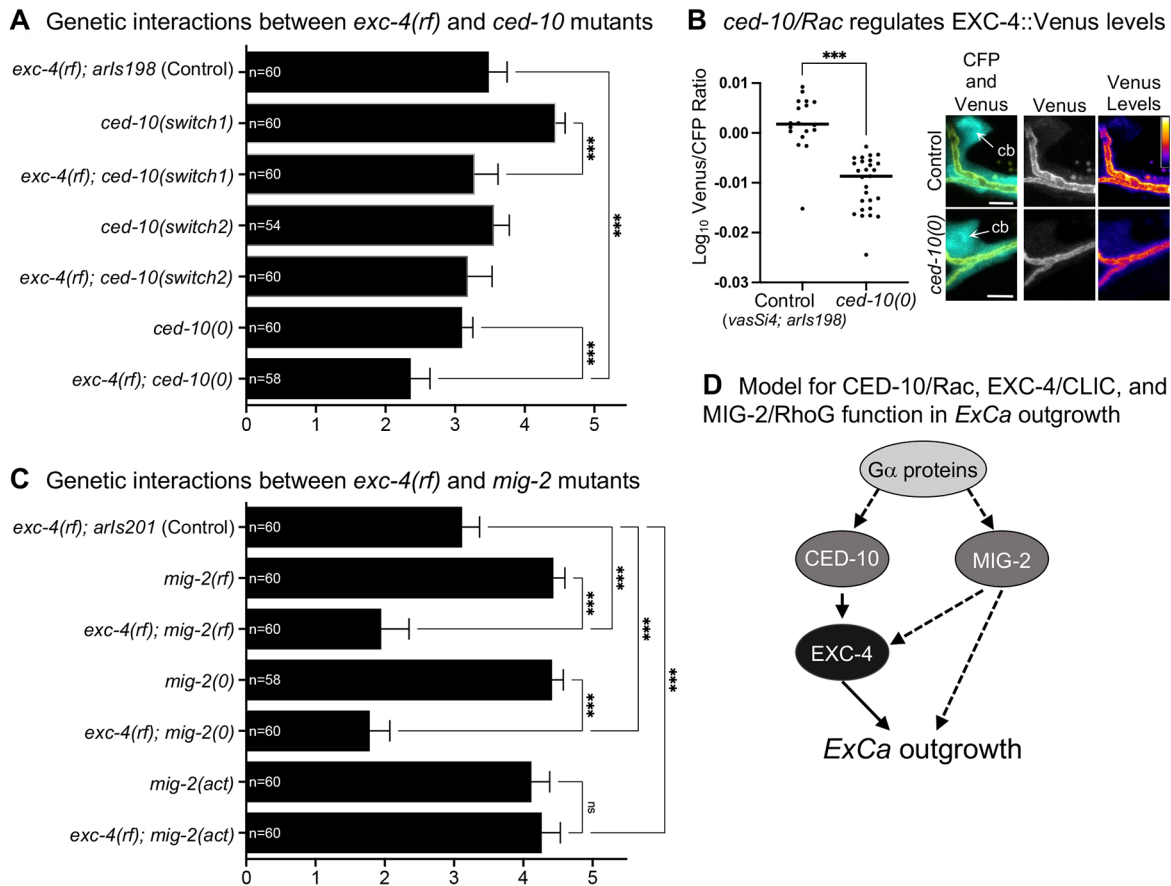


Fig. 5. *ced-10* regulates *exc-4* expression, and *mig-2* functions in parallel. (A) Combining *exc-4(rf)* with the *ced-10* loss-of-function alleles, *ced-10(rp100)* or *ced-10(n3246)*, does not exacerbate the *exc-4(rf)* ExCa outgrowth phenotype, consistent with function in a single pathway. However, combining *exc-4(rf)* and *ced-10(n3417)* causes a more severe phenotype, raising possibility that *ced-10* and *exc-4* function, for some aspects of ExCa outgrowth, in parallel. (B) *ced-10* promotes EXC-4::Venus accumulation. Each dot in the plot represents a single ~5 μm^2 region of interest from a single 0.5 μm z-section, measured for CFP and Venus fluorescence (see Materials and Methods). At least eight animals of each genotype were analyzed, and we note that cytoplasmic CFP levels were not significantly affected by *ced-10* loss. Images on the right are representative maximum-intensity z-projections taken near the ExCa cell body (cb). Scale bars: 5 μm . (C) Mutations that reduce or eliminate *mig-2* function, *mig-2(gm38)* or *mig-2(mu28)*, respectively, enhance the *exc-4(rf)* outgrowth defect, whereas an activated allele, *mig-2(gm103)*, suppresses *exc-4(rf)*. See Table S1 for full genotypes. In the graphs, solid bars show average posterior ExCa outgrowth (see Materials and Methods) and error bars are the 95% confidence interval. One-way ANOVA with Bonferroni correction for multiple comparisons was used to calculate significance; *** $P < 0.001$. ns, not significant. (D) Speculative model of $G\alpha$, CED-10, MIG-2 and EXC-4 function in ExCa outgrowth. $G\alpha$ proteins typically act upstream, and as positive regulators, of Rho/Rac proteins (Kjoller and Hall, 1999). Therefore, we tentatively place the function of *egl-30/G α_q* , *gpa-12/G $\alpha_{12/13}$* , *gsa-1/G α_s* and *gpa-7/G α_i* upstream of *ced-10* and/or *mig-2* in ExCa outgrowth. Genetic evidence and rescue experiments (Fig. 4) support a model in which *ced-10* and *mig-2* act in parallel in the ExCa to promote outgrowth, and regulation of EXC-4::Venus by *ced-10* suggests that *exc-4* is regulated by, and functions downstream of, *ced-10*. Finally, genetic interactions between *mig-2* mutants and *exc-4(rf)* are consistent with a model in which *mig-2* acts upstream of, or in parallel to, *exc-4* to regulate ExCa outgrowth.

ExCa (Fig. 4) further highlights the molecular and mechanistic similarities between neuronal and ExCa outgrowth (reviewed by Sundaram and Buechner, 2016; Shaye and Soto, 2021).

CED-10 regulates the levels of EXC-4 in the ExCa

We note that, as in *exc-4(rf)* mutants, cystic ExCa were not seen in *ced-10* or *mig-2* single mutants (Fig. 4B; data not shown), or in the stronger *ced-10*; *mig-2* double mutants (Fig. 4D), leading us to hypothesize that *ced-10* and/or *mig-2* function in the same pathway as *exc-4* in ExCa outgrowth. To assess the functional relationship between these genes, we investigated genetic interactions among them by constructing strains carrying different combination of mutants in these genes. Attempts to combine *exc-4(0)* with *ced-10* or *mig-2* mutations resulted in severe sickness and/or lethality. Therefore, we instead evaluated genetic interactions using the *exc-4(rf)* mutation, as we did above for $G\alpha$ -encoding genes.

We found that combining *exc-4(rf)* with the weaker *ced-10(switch1)* or *ced-10(switch2)* alleles did not modify the *exc-4(rf)* outgrowth defect, whereas combining *exc-4(rf)* with *ced-10(0)* enhanced the outgrowth defect of both mutants, indicating that *exc-4* and *ced-10* genetically interact. Because *exc-4(rf)* is a non-null allele, genetic interactions results do not illuminate the order of *exc-4* and *ced-10* function. However, previous work in cultured endothelial cells showed that RhoA activity promotes apical accumulation of CLIC4 (Ponsioen et al., 2009), so we investigated whether CED-10 similarly functions upstream of EXC-4 to regulate its accumulation. To avoid unwanted effects due to overexpression, we created a single-copy insertion transgene expressing EXC-4::Venus in the ExCa (*vasSi4*) and visualized Venus levels in wild type and in *ced-10(0)* mutants. To quantify expression, we normalized Venus levels to cytoplasmic CFP (expressed from the integrated array *arIs198*) in each background, and found that *ced-10* loss significantly reduced EXC-4::Venus

levels (Fig. 5B). This reduction is not an effect of *ced-10(0)* on the *glt-3p* promoter, as we did not see a significant change in CFP expression from *arl-198*, which also uses the same promoter (Fig. S6A). This result suggests that CED-10 functions upstream of EXC-4 to promote its accumulation in the ExCa.

We showed above that *ced-10* and *mig-2* function in parallel to promote ExCa outgrowth (Fig. 4D). If *ced-10* and *exc-4* function in the same pathway, then we expect that combining *exc-4(rf)* with *mig-2* loss-of-function mutations should cause enhanced phenotypes, like those seen in *ced-10; mig-2* double loss-of-function mutant strains (Fig. 4D). We constructed *exc-4(rf); mig-2(rf)* and *exc-4(rf); mig-2(0)* double mutants, and indeed found that these animals displayed a stronger phenotype than the respective singles (Fig. 5C). In addition, when we combined *exc-4(rf)* with the activated *mig-2(act)* allele we saw robust suppression of the *exc-4(rf)* outgrowth phenotype (Fig. 5C). Because the *exc-4(rf)* allele is non-null, several interpretations of these genetic interactions are possible. One is that *mig-2* functions downstream of the proposed *ced-10* and *exc-4* pathway, and thus activating *mig-2* compensates for reduced *exc-4* function. However, because we have evidence, using null alleles, that *ced-10* and *mig-2* function in parallel (Fig. 4D), instead of *mig-2* acting downstream of the proposed *ced-10–exc-4* pathway, we favor a model in which *mig-2* functions upstream of, or in parallel to, *exc-4* to promote ExCa outgrowth (Fig. 5D). Unfortunately, we were unable to assess effects of *mig-2* loss, or activation, on EXC-4::Venus levels to determine whether *mig-2* functions upstream of *exc-4*, like we did for *ced-10* (Fig. 4B), because *mig-2* mutations affected expression from the *glt-3p* promoter used to drive EXC-4::Venus (Fig. S6B).

DISCUSSION

Our discovery of an *exc-4* mutation that affects a metazoan-specific motif, not found in GST- Ω proteins nor in bacterial or plant CLIC-like proteins with ion channel activity, revealed a new function for EXC-4/CLIC in cell outgrowth. This new *exc-4* mutant also allowed us to demonstrate, using genetic interactions, that the emerging function for CLICs in G α and Rho/Rac signaling is conserved and that this pathway regulates cell outgrowth during tubulogenesis *in vivo*.

A new mutation reveals a specific function for EXC-4 in cell outgrowth

We identified a new *exc-4* loss-of-function mutation using the *C. elegans* ‘Million Mutation Project’: an effort that has generated a collection of random, viable and well-annotated mutants (Thompson et al., 2013). Our finding that *exc-4(rf)* causes ExCa shortening without the formation of large cysts is in contrast with the previously described, all likely null, *exc-4* mutants (Buechner et al., 1999; Berry et al., 2003). The finding that EXC-4 Cys237 is required for ExCa outgrowth, but does not play a significant role in lumen diameter maintenance, leads us to propose that EXC-4/CLICs have discrete and separable functions in tubulogenesis. We also found that EXC-4 Cys237 is not required for protein localization to the apical plasma membrane, and, to our knowledge, this is the first report of a mutation affecting CLIC function without disrupting localization (e.g. see Berry and Hobert, 2006; Al-Momany et al., 2014). GPCR-induced cytoplasmic-to-plasma membrane re-localization of CLIC4 in cultured cells was unaffected by mutation of the equivalent cysteine, CLIC4^{C234} (Ponsioen et al., 2009), consistent with our findings. However, as assays for GPCR-induced CLIC4 functions were not available at the time, Ponsioen et al. (2009) could not assess the functional relevance of this cysteine. Our work highlights the utility of a resource such as the ‘Million Mutation Project’, which,

combined with the power of genetic analysis in *C. elegans*, allowed us to define a previously unappreciated and physiologically relevant cellular function for EXC-4/CLICs.

EXC-4 Cys237 resides in a profoundly conserved motif unrelated to CLIC ion channel or GST activities

EXC-4 Cys237 resides within a motif (consensus FxxTCxxDx[D/E]Ixxx[W/Y], where the relevant Cys is bold and underlined) found at the C terminus of metazoan CLICs. As this cysteine and the surrounding motif are not present in GST- Ω proteins, nor in bacterial or plant CLIC-like proteins with ion channel activity (Elter et al., 2007; Gururaja Rao et al., 2017), we conclude that this motif is unrelated to the GST or ion channel activities often ascribed to CLICs. Thus, we propose that CLIC function in cell outgrowth relies on an unknown activity residing within this C-terminal motif. We also note that GST- Ω , non-metazoan CLIC-like proteins (including those from choanoflagellates, the closest unicellular relatives to metazoans), and the most diverged metazoan protein, *A. queenslandica* CLIC, lack, or have a degenerate, N-terminal PTMD. Because the PTMD (Berry et al., 2003; Berry and Hobert, 2006) and C-terminal cysteine (our work here) are required for EXC-4 function in the ExCa, we speculate that these two features endow CLICs with a function in cell outgrowth that arose in multicellular organisms. Our sequence and phylogenetic analysis of GST- Ω and CLIC proteins not only provides insight into the evolutionary history of CLICs, but should help guide future structure-function studies to decipher EXC-4/CLIC regulation and function.

EXC-4 functions with G α and Rho/Rac signaling in the ExCa to mediate outgrowth

Cell culture studies have demonstrated that CLICs function in GPCR-G α / β / γ -Rho/Rac signaling (Ponsioen et al., 2009; Tavasoli et al., 2016b; Argenzio et al., 2018; Mao et al., 2021). We now extend these findings by showing that G α proteins, CED-10, MIG-2 and EXC-4 work together to regulate a cellular behavior, ExCa outgrowth, in a physiological setting. Therefore, our work shows that CLIC function in G α and Rho/Rac signaling is evolutionarily conserved and required for tubulogenesis during development.

Where, and how, CLICs function in G α and Rho/Rac signaling remains an open question. Some studies have placed G α and Rho/Rac function upstream of CLICs (Ponsioen et al., 2009; Argenzio et al., 2018), whereas others show instead that CLICs function upstream of, and activate, Rho/Rac GTPases (Tavasoli et al., 2016b; Mao et al., 2021). Our genetic and expression studies suggest that CED-10 acts upstream of EXC-4, whereas our genetic interaction results are consistent with MIG-2 functioning in a parallel pathway, either via *exc-4* or in an independent manner (Fig. 5D). Our genetic results also implicate *egl-30/G α_q* , *gpa-12/G $\alpha_{12/13}$* , *gsa-1/G α_s* , and *gpa-7/G α_i* in ExCa outgrowth; however, they do not allow us to define the precise functional relationship between these G α proteins and EXC-4. We note that G α proteins typically act upstream of Rho/Rac GTPases (Kj  ller and Hall, 1999); thus, it is possible that the genetic interactions observed between G α -encoding genes and *exc-4* occur via G α -mediated regulation of *ced-10* and/or *mig-2*. Deciphering the precise functional relationship between G α proteins, CED-10 and MIG-2 in ExCa outgrowth will be difficult owing to redundancy among G α -encoding genes, suggested by the fact that single, double and triple mutant combinations of G α -encoding genes do not result in ExCa phenotypes, which could be further exacerbated by the redundancy between *ced-10* and *mig-2* that we describe here.

Because mutations in *ced-10* and *mig-2* caused ExCa outgrowth defects without an accompanying cystic phenotype, and because

ced-10 functions in the same pathway as *exc-4*, we propose that CED-10 is involved in the cell outgrowth function of EXC-4 mediated by the EXC-4 Cys237 residue. We speculate that further analysis of this motif will reveal how Gα and Rho/Rac pathways interface with EXC-4/CLICs, and help us to understand the emerging signaling function for this enigmatic protein family that is crucial for tubulogenesis and vascular biology.

MATERIALS AND METHODS

Strains

Standard methods were used for strain handling and maintenance (Brenner, 1974). Animals were grown at 20°C, unless otherwise noted. Full genotypes for all strains are listed in Table S1, and mutant alleles are described in WormBase (www.wormbase.org). Primers (Sigma-Aldrich) used for genotyping are listed in Table S2. Fluorescent transgenes to visualize the ExCa, or used in crosses and/or to maintain sterile or lethal mutants (described by Frøkjær-Jensen et al., 2014; Dejima et al., 2018, unless otherwise noted), were: Linkage Group (LG)1: *oxTi550*, *oxTi559*, *oxTi718*, *oxTi723*, *tmC20[Venus]*; LG3: *rhIs4* (Hsieh et al., 1999); LG4: *oxTi608*, *oxTi915*, *oxTi404*, *oxTi554*, *tmC25[Venus]*, *arIs201* [this work; made as previously described for *arIs198* in Shaye and Greenwald (2015)]; LG5: *oxTi575*, *oxTi405*, *arIs164* (Shaye and Greenwald, 2015); LGX: *oxTi400*, *tmC24[mCherry]*, *arIs198* (Shaye and Greenwald, 2015).

To identify *exc-4(rf)*, we scanned the ‘Million Mutation Project’ database (Thompson et al., 2013) for mutations that changed amino acids conserved between *C. elegans* EXC-4, *Drosophila* CLIC, and human CLIC1, 4 and 5. Four candidate mutations were outcrossed at least three times into a strain carrying the ExCa marker *arIs198* (Shaye and Greenwald, 2015) to remove background mutations and score ExCa phenotypes. Two candidate mutations failed to complement the *exc-4* null mutant: *exc-4(565032)*, a mutation changing EXC-4^{A55} to Glu, and *exc-4(gk451333)*, a mutation changing EXC-4 Cys237 to Tyr (Fig. 1B,C). However, only *exc-4(gk451333)* caused significant ExCa phenotypes when homozygous; thus, we referred to it as *exc-4(rf)* and used this allele for the studies described here.

Plasmids and transgenes

Standard molecular biology techniques were used to generate plasmids for transgenesis, and details of plasmid construction can be found in the supplementary Materials and Methods. Primers (listed in Table S2) were from Sigma-Aldrich, and dsDNA ‘geneblocks’ (gBlocks; see Table S3) were from IDT. All plasmids were sequenced-verified by Sanger sequencing performed at UIC’s Research Resources Center sequencing core.

Multi-copy extrachromosomal transgenes were generated by microinjection (Evans, 2006). Multi-copy integrated transgenes (*arIs190*, *vasIs2*) were generated by X-ray irradiation and MiniSOG-mediated integration, respectively (reviewed in Nance and Frøkjær-Jensen, 2019). Mos1 and CRISPR-based approaches (reviewed by Nance and Frøkjær-Jensen, 2019) were used to generate single-copy, genome-inserted transgenes. The randomly integrated single-copy transgene *vasTi2* was mapped as described (Frøkjær-Jensen et al., 2014). The location and integrity of the single-copy genomic insertions *vasSi1*, *vasSi4*, *vasSi11*, *vasSi16* and *vasTi2* were verified by PCR and sequencing of genomic DNA from transgenic animals.

Integrated multi-copy array *arIs190[glt-3p::exc-4::Venus]*

We first created the extrachromosomal array *arEx1333* by injecting plasmid pDS335 (20 ng/μl), carrying *glt-3p::exc-4::Venus* and *Caenorhabditis briggsae unc-119(+)* sequences that rescue *unc-119* mutants (Maduro and Pilgrim, 1996), and pBluescript (pBS) DNA (80 ng/μl) as ‘filler’, into *unc-119(ed3)* animals. This extrachromosomal array was integrated by X-ray irradiation as described (Evans, 2006) and outcrossed to wild type at least four times to remove background mutations.

Integrated multi-copy array *vasIs2[glt-3p::exc-4^{C237Y}::Venus]*

Plasmid pAA15 (20 ng/μl), encoding *glt-3p::exc-4^{C237Y}::Venus*, pNC4.21 (30 ng/μl), which rescues *unc-4* mutants (Miller and Niemeyer, 1995), and

pBS (50 ng/μl) as ‘filler’ into *unc-4(e120); juSi164 unc-119(ed3)* animals. The transgene *juSi164* in this background expresses H2B-MiniSOG in the germline, which creates double-stranded DNA breaks upon exposure to blue light (Noma and Jin, 2016). Injected animals were exposed to blue light ~6 h after injection and *unc-4*-rescued animals were singled to isolate integrants. The multi-copy array *vasIs2* was crossed out of the *unc-4(e120); juSi164 unc-119(ed3)* background and outcrossed at least four times to wild type to remove background mutations.

Multicopy extrachromosomal array *vasEx34[glt-3p::mScarlet(l)::3xFLAG::ced-10]*

This transgene was generated, as described above, using a mix containing 5 ng/μl of plasmid pAA54 (*glt-3p::mScarlet(l)::3xFLAG::ced-10*), 2.5 ng/μl pCFJ90 [*myo-2p::mCherry*; a gift from Erik Jorgensen (Addgene plasmid #19327)] and 50 ng/μl each of the *pha-1(+)* plasmid pBX and the Hygro^R plasmid pIR98 (both described above).

Single-copy insertion *vasSi1[glt-3p::Venus]*

Plasmid pAA8, containing *glt-3p::Venus* and a self-excising selection cassette (SEC; see Dickinson et al., 2015) flanked by homology to the LG1 locus *ttTi4348* (Frøkjær-Jensen, 2015), was linearized with PciI and mixed, to a final concentration of 7 ng/μl, with pCas9 (Cas9-expressing plasmid, a gift from A. Pani, D. Matus and B. Goldstein, University of North Carolina, Chapel Hill, USA; 50 ng/μl), 5 μM of single-guide RNA (sgRNA, Synthego) targeting *ttTi4348*, and the co-injection markers pCFJ90 (described above) and pGH8 [*rab-3p::mCherry*, 5 ng/μl; a gift from Erik Jorgensen (Addgene plasmid #19359)]. This mix was injected into wild-type (N2) hermaphrodites. After injection-transformed animals and the resulting single-copy insertion were selected, the SEC was excised, as described (Dickinson et al., 2015).

Single-copy insertions *vasSi4[glt-3p::exc-4::Venus]*, *vasSi11[glt-3p::exc-4(opt)]* and *vasSi16[glt-3p::exc-4^{C237Y}(opt)]*

These single-copy insertions were generated using the MosSCI approach (Frøkjær-Jensen, 2015). We used single-copy insertions for rescue experiments to avoid confounding effects caused by protein overexpression. Moreover, the MosSCI technique allows for insertion of transgenes at an identical known site, thereby alleviating differences between transgenes that could be due to positional effects. However, we found that single-copy insertions of the wild-type *exc-4* cDNA did not rescue *exc-4(0)* as efficiently as multi-copy transgenes carrying the same sequence, likely due to lower expression levels. Therefore, we generated *exc-4(opt)*, a codon-optimized cDNA that includes a synthetic intron, known to optimize expression in *C. elegans* (Redemann et al., 2011), and used this cDNA (obtained from IDT as a dsDNA gBlock; see Table S3 for sequence) for the rescue experiments shown in Fig. 1E-G.

Constructs of interest were cloned into plasmid pJE24, which carries a hygromycin-resistance (Hygro^R) cassette and multiple-cloning site flanked by homology to the LG1 locus *ttTi4348* (Frøkjær-Jensen, 2015). Mixes containing plasmid pJE43 (*ttTi4348[glt-3p::exc-4::Venus]*), pJE51 (*ttTi4348[glt-3p::exc-4(opt)]*) or pAA70 (*ttTi4348[glt-3p::exc-4^{C237Y}(opt)]*), at 50 ng/μl, as well as pCFJ90 (*myo-2p::mCherry*, described above), pCFJ2475 (*smu-2p::Mos1transposase(PATCS)::smu-1 3'UTR*; described by Aljohani et al., 2020; Addgene #159813) at 15 ng/μl, and pSEM238 (*snt-1p::ce-HisC11*, encoding a histamine-gated chloride channel expressed in the nervous system; described by El Mouridi et al. (2021); Addgene #161515) at 20 ng/μl, and pBS at 12.5 ng/μl were injected into animals carrying the Mos1 transposon *ttTi4348*. Integrants were identified as hygromycin-resistant animals that lost extrachromosomal array markers (i.e. were *myo-2p::mCherry* negative and were not paralyzed on histamine; an indication that they do not carry *snt-1p::ce-HisC11*).

Single-copy insertion *vasTi2[glt-3p::FLAG::ced-10]*

This transgene was made using the miniMos protocol for random single-copy genome insertions (Frøkjær-Jensen et al., 2014). A mix containing pAA42, which is neomycin resistant (10 ng/μl), pCFJ90 (described above),

pMA122 (*hsp16.41::peel-1::tbb-2* 3' UTR, 20 ng/μl) and pCFJ601 (*eft-3::Mos1* transposase::tbb-2 3' UTR, 130 ng/μl), gifts from Erik Jorgensen (Addgene plasmids #34873, #34874), was injected into N2 hermaphrodites and transformants were selected by *myo-2::mCherry* and growth on neomycin. Heat-shock to drive expression of the toxic protein PEEL-1 was used to select against extrachromosomal arrays and identify the neomycin-resistant insertion *vasTi2*.

Imaging

Animals were mounted on 5% agar and immobilized with 2.5 mM levamisole followed by immediate imaging. For scoring outgrowth phenotypes, animals were imaged on Zeiss AxioImager Z2 using a 20× objective. For confocal imaging (Fig. 1D), we visualized Venus and CFP from transgenes *vasSi1*, *vasEx1* and *vasIs2* using a 40× water immersion objective mounted on a Zeiss LSM880 confocal system with AiryScan acquisition. For CFP (458 nm), laser power was 2.0, 2.6 and 2.0% for each transgene, respectively, as listed above. For Venus (514 nm), laser power was 2.2, 2.0 and 2.2%, for each transgene. Gain was equivalent for all images, with CFP=1000 and Venus=932. Images were AiryScan-processed and post-processed with ImageJ using identical settings for all.

Quantification of EXC-4::Venus levels in control and *ced-10(0)* mutants

Control (*vasSi4*; *arIs198*) and *vasSi4*; *ced-10(0)*; *arIs198* animals were grown at 22°C in parallel. Larvae were mounted and filmed by AiryScan confocal microscopy as described above. Acquisition settings for all genotypes were: CFP (445 nm) laser power at 3.3%, EM gain 600, and exposure 100 ms; YFP (514 nm) laser power at 10.8%, EM gain 570, exposure 300 ms. We used Fiji/ImageJ to measure CFP and Venus levels in 5 μm² regions ($n \geq 8$ ExCa per genotype, at a similar area near the cell body for all) of single 0.5-μm-thick z-sections. For ease of viewing, representative images shown in Fig. 5B are maximum-intensity z-projections; however, quantification was carried out on single z-sections to avoid additive effects caused by z-projections.

Scoring ExCa outgrowth and cystic phenotypes

The ExCa was visualized with *arIs164*, expressing cytoplasmic Venus, and *arIs198* or *arIs201*, both expressing cytoplasmic CFP and apically localized LifeAct-TagRFP (Shaye and Greenwald, 2015, 2016). Wild-type animals carrying these transgenes were used as controls. Each ExCa arm grows independently (Shaye and Greenwald, 2015, 2016), so we scored outgrowth of each posterior canal in distinct animals independently. We were not able to blind researchers as to the genotypes being scored, because most mutations used display pleiotropies making it difficult to remain blinded to the underlying genotypes. We do note that many of the backgrounds here were constructed and/or viewed by at least two of the authors, and others in the lab, with none reporting obvious deviations from the reported phenotypes. We used morphological landmarks (see Fig. 1A,B) to assign an 'outgrowth score' (0-5; see Fig. 1B, control) to each posterior canal. A score of '0' indicates no outgrowth, '3' indicates outgrowth to the vulva and '5' indicates outgrowth to the rectum. We assigned each animal a 'cystic score' (0-4; see Fig. 1B, control), with '0' indicating animals with no cysts, or only small swellings, '1' animals with cyst size approximately a quarter of the body width, '2' with cysts between a quarter and half of the body width, '3' cysts approximately three-quarters of the body width, and '4' if the cyst encompassed the entire width of the body. We used GraphPad Prism software to run statistical tests and generate graphs. Statistical details are given in each figure legend.

Sequence alignment and phylogenetic analysis

C. elegans EXC-4 and GST-44 were used as queries for BLASTP searches (Altschul et al., 1990) at the NIH-NIMH (<https://blast.ncbi.nlm.nih.gov/Blast.cgi>) non-redundant protein database, and at the Uniprot (<https://www.uniprot.org/blast/>) KB database, using default parameters. After we identified putative CLICs from *A. queenslandica*, *T. adhaerens* and *N. vectensis*, we also used these as queries in further BLASTP searches to ensure that we did not miss highly divergent orthologs. However, these

searches did not identify further CLIC orthologs in more diverged species. For vertebrate CLICs, we restricted our analysis to one mammalian (*Homo sapiens*) and one non-mammalian (*Danio rerio*) species and focused on the endothelial-expressed CLICs (CLIC1, 4 and 5a). In species in which more than one putative CLIC ortholog was identified by BLASTP, we restricted our analysis to the paralog with highest sequence similarity to EXC-4.

We aligned the full-length sequences of GSTΩs, CLICs and the functionally distinct yeast glutathione-S-transferase Gtt2p (Choi et al., 1998; Ma et al., 2009), which we used as an outgroup in phylogenetic tree construction (see below), using the CLUSTALW algorithm (Thompson et al., 1994) in the MacVector software package (MacVector, Inc.) with default settings (Gonnet matrix, Open Gap Penalty=10; Extended Gap Penalty=0.2, Delay Divergent=30%). To ensure that absence of the C-terminal cysteine in four, out of 20, metazoan CLICs (those from *T. adhaerens*, sea urchin, oyster and amphioxus; see Fig. 2A) indicates a true evolutionary loss, and not a sequencing error or under-sampling, we used BLASTP to search for CLICs in other species within the same phylum, or sub-phylum, as these four species. Unfortunately, *T. adhaerens* is the only Placozoan sequenced to date, but we identified putative CLICs in six additional echinoderms, 56 additional mollusks and one additional cephalochordate, and these also lacked the C-terminal cysteine. This suggests that this residue was truly lost in echinoderm, mollusk and cephalochordate lineages. We used MacVector to create a phylogenetic tree (Fig. S3) via the Neighbor-joining method with the following settings: bootstrap=5000, random tie breaking among equivalent trees, uncorrected distance ('p'), and proportional gap distribution.

Acknowledgements

We would like to thank Iva Greenwald, Jan Kitajewski, Alexandra Socovich and Claire Bénard for comments. We are grateful to Raphaël Dima and Claire Bénard (UQAM) for sharing unpublished data and reagents, and to Jan Kitajewski, De Yu Mao and Matt Kleinjan (UIC) for helpful discussions. We also thank Alison Kitajewski for technical assistance, Roger Pocock (Monash University) for the *ced-10(knu268)* strain, the UIC Research Resource Center core facilities and the *Caenorhabditis* Genetics Center (CGC, University of Minnesota), funded by the NIH Office of Research Infrastructure Programs (P40 OD010440), for strains.

Competing interests

The authors declare no competing or financial interests.

Author contributions

Conceptualization: A.F.A., D.D.S.; Methodology: A.F.A., D.D.S.; Validation: A.F.A.; Formal analysis: A.F.A., J.E., D.D.S.; Investigation: A.F.A., J.E.; Resources: J.E., D.D.S.; Data curation: A.F.A.; Writing - original draft: A.F.A., D.D.S.; Writing - review & editing: A.F.A., D.D.S.; Visualization: A.F.A., J.E.; Supervision: D.D.S.; Project administration: D.D.S.; Funding acquisition: A.F.A., D.D.S.

Funding

This study was supported by a National Science Foundation Graduate Research Fellowship Program grant (1444315 to A.F.A.), a L@S GANAS fellowship funded by the United States Department of Education (HSI-STEM; P031C160237 to J.E.), a 'Research Supplement to Promote Diversity' from the National Heart, Lung, and Blood Institute (NHLBI R01HL119403-02S1) and the National Institute of General Medical Sciences (R01 GM134032 to D.D.S.). Early stages of this work were supported by Iva Greenwald (Howard Hughes Medical Institute and Columbia University). Deposited in PMC for release after 12 months.

References

- Adams, R. H. and Eichmann, A. (2010). Axon guidance molecules in vascular patterning. *Cold Spring Harb. Perspect. Biol.* **2**, a001875. doi:10.1101/cshperspect.a001875
- Al-Momany, A., Li, L., Alexander, R. T. and Ballermann, B. J. (2014). Clustered PI(4,5)P(2) accumulation and ezrin phosphorylation in response to CLIC5A. *J. Cell Sci.* **127**, 5164-5178. doi:10.1242/jcs.147744
- Aljohani, M. D., El Mouridi, S., Priyadarshini, M., Vargas-Velazquez, A. M. and Frøkjær-Jensen, C. (2020). Engineering rules that minimize germline silencing of transgenes in simple extrachromosomal arrays in *C. elegans*. *Nat. Commun.* **11**, 6300. doi:10.1038/s41467-020-19898-0
- Altschul, S. F., Gish, W., Miller, W., Myers, E. W. and Lipman, D. J. (1990). Basic local alignment search tool. *J. Mol. Biol.* **215**, 403-410. doi:10.1016/S0022-2836(05)80360-2

- Argenzio, E. and Moolenaar, W. H. (2016). Emerging biological roles of Cl⁻ intracellular channel proteins. *J. Cell Sci.* **129**, 4165-4174. doi:10.1242/jcs.189795
- Argenzio, E., Klarenbeek, J., Kedziora, K. M., Nahidiazar, L., Isogai, T., Perrakis, A., Jalink, K., Moolenaar, W. H. and Innocenti, M. (2018). Profilin binding couples chloride intracellular channel protein CLIC4 to RhoA-mDia2 signaling and filopodium formation. *J. Biol. Chem.* **293**, 19161-19176. doi:10.1074/jbc.RA118.002779
- Bastiani, C. and Mendel, J. (2006). Heterotrimeric G proteins in *C. elegans*. *WormBook*. **13**, 1-25. doi:10.1895/wormbook.1.75.1
- Bergmann, D. C., Lee, M., Robertson, B., Tsou, M.-F. B., Rose, L. S. and Wood, W. B. (2003). Embryonic handedness choice in *C. elegans* involves the G α protein GPA-16. *Development* **130**, 5731-5740. doi:10.1242/dev.00839
- Berman, H. M., Westbrook, J., Feng, Z., Gilliland, G., Bhat, T. N., Weissig, H., Shindyalov, I. N. and Bourne, P. E. (2000). The protein data bank. *Nucleic Acids Res.* **28**, 235-242. doi:10.1093/nar/28.1.235
- Berry, K. L. and Hobert, O. (2006). Mapping functional domains of chloride intracellular channel (CLIC) proteins *in vivo*. *J. Mol. Biol.* **359**, 1316-1333. doi:10.1016/j.jmb.2006.04.046
- Berry, K. L., Bülow, H. E., Hall, D. H. and Hobert, O. (2003). A *C. elegans* CLIC-like protein required for intracellular tube formation and maintenance. *Science* **302**, 2134-2137. doi:10.1126/science.1087667
- Betz, C., Lenard, A., Belting, H.-G. and Affolter, M. (2016). Cell behaviors and dynamics during angiogenesis. *Development* **143**, 2249-2260. doi:10.1242/dev.135616
- Board, P. G., Coggan, M., Chelvanayagam, G., Easteal, S., Jermini, L. S., Schulte, G. K., Danley, D. E., Hoth, L. R., Griffor, M. C., Kamath, A. V. et al. (2000). Identification, characterization, and crystal structure of the omega class glutathione transferases. *J. Biol. Chem.* **275**, 24798-24806. doi:10.1074/jbc.M001706200
- Bohman, S., Matsumoto, T., Suh, K., Dimberg, A., Jakobsson, L., Yuspa, S. and Claesson-Welsh, L. (2005). Proteomic analysis of vascular endothelial growth factor-induced endothelial cell differentiation reveals a role for chloride intracellular channel 4 (CLIC4) in tubular morphogenesis. *J. Biol. Chem.* **280**, 42397-42404. doi:10.1074/jbc.M506724200
- Brenner, S. (1974). The genetics of *Caenorhabditis elegans*. *Genetics* **77**, 71-94. doi:10.1093/genetics/77.1.71
- Brundage, L., Avery, L., Katz, A., Kim, U.-J., Mendel, J. E., Sternberg, P. W. and Simon, M. I. (1996). Mutations in a *C. elegans* G α gene disrupt movement, egg laying, and viability. *Neuron* **16**, 999-1009. doi:10.1016/S0896-6273(00)80123-3
- Buechner, M., Hall, D. H., Bhatt, H. and Hedgecock, E. M. (1999). Cystic canal mutants in *Caenorhabditis elegans* are defective in the apical membrane domain of the renal (excretory) cell. *Dev. Biol.* **214**, 227-241. doi:10.1006/dbio.1999.9398
- Burley, S. K., Bhikadiya, C., Bi, C., Bittrich, S., Chen, L., Crichlow, G. V., Christie, C. H., Dalenberg, K., Di Costanzo, L., Duarte, J. M. et al. (2021). RCSB Protein Data Bank: powerful new tools for exploring 3D structures of biological macromolecules for basic and applied research and education in fundamental biology, biomedicine, biotechnology, bioengineering and energy sciences. *Nucleic Acids Res.* **49**, D437-D451. doi:10.1093/nar/gkaa1038
- Choe, K. P. and Strange, K. (2007). Evolutionarily conserved WNK and Ste20 kinases are essential for acute volume recovery and survival after hypertonic shrinkage in *Caenorhabditis elegans*. *Am. J. Physiol. Cell Physiol.* **293**, C915-C927. doi:10.1152/ajpcell.00126.2007
- Choi, J. H., Lou, W. and Vancura, A. (1998). A novel membrane-bound glutathione S-transferase functions in the stationary phase of the yeast *Saccharomyces cerevisiae*. *J. Biol. Chem.* **273**, 29915-29922. doi:10.1074/jbc.273.45.29915
- Dbouk, H. A., Weil, L. M., Perera, G. K. S., Dellinger, M. T., Pearson, G., Brekken, R. A. and Cobb, M. H. (2014). Actions of the protein kinase WNK1 on endothelial cells are differentially mediated by its substrate kinases OSR1 and SPAK. *Proc. Natl. Acad. Sci. USA* **111**, 15999-16004. doi:10.1073/pnas.1419057111
- deBakker, C. D., Haney, L. B., Kinchen, J. M., Grimsley, C., Lu, M., Klingele, D., Hsu, P.-K., Chou, B.-K., Cheng, L.-C., Blangy, A. et al. (2004). Phagocytosis of apoptotic cells is regulated by a UNC-73/TRIO-MIG-2/RhoG signaling module and armadillo repeats of CED-12/ELMO. *Curr. Biol.* **14**, 2208-2216. doi:10.1016/j.cub.2004.12.029
- Dejima, K., Hori, S., Iwata, S., Suehiro, Y., Yoshina, S., Motohashi, T. and Mitani, S. (2018). An aneuploidy-free and structurally defined balancer chromosome toolkit for *Caenorhabditis elegans*. *Cell Rep.* **22**, 232-241. doi:10.1016/j.celrep.2017.12.024
- Dickinson, D. J., Pani, A. M., Heppert, J. K., Higgins, C. D. and Goldstein, B. (2015). Streamlined genome engineering with a self-excising drug selection cassette. *Genetics* **200**, 1035-1049. doi:10.1534/genetics.115.178335
- El Mouridi, S., Alharbi, S. and Frøkjær-Jensen, C. (2021). A histamine-gated channel is an efficient negative selection marker for *C. elegans* transgenesis. *MicroPubl. Biol.* **2021**. doi:10.17912/micropub.biology.000349
- Elter, A., Hartel, A., Sieben, C., Hertel, B., Fischer-Schliebs, E., Lüttge, U., Moroni, A. and Thiel, G. (2007). A plant homolog of animal chloride intracellular channels (CLICs) generates an ion conductance in heterologous systems. *J. Biol. Chem.* **282**, 8786-8792. doi:10.1074/jbc.M607241200
- Evans, T. (2006). Transformation and microinjection. *WormBook* **6**, 1-15. doi:10.1895/wormbook.1.108.1
- Forrester, W. C. and Garriga, G. (1997). Genes necessary for *C. elegans* cell and growth cone migrations. *Development* **124**, 1831-1843. doi:10.1242/dev.124.9.1831
- Forrester, W. C., Perens, E., Zallen, J. A. and Garriga, G. (1998). Identification of *Caenorhabditis elegans* genes required for neuronal differentiation and migration. *Genetics* **148**, 151-165. doi:10.1093/genetics/148.1.151
- Fredriksson, R., Lagerström, M. C., Lundin, L.-G. and Schiöth, H. B. (2003). The G-protein-coupled receptors in the human genome form five main families. Phylogenetic analysis, paralogon groups, and fingerprints. *Mol. Pharmacol.* **63**, 1256-1272. doi:10.1124/mol.63.6.1256
- Frøkjær-Jensen, C. (2015). Transposon-assisted genetic engineering with mos1-mediated single-copy insertion (MosSCI). *Methods Mol. Biol.* **1327**, 49-58. doi:10.1007/978-1-4939-2842-2_5
- Frøkjær-Jensen, C., Davis, M. W., Sarov, M., Taylor, J., Flibotte, S., LaBella, M., Pozniakovsky, A., Moerman, D. G. and Jorgensen, E. M. (2014). Random and targeted transgene insertion in *Caenorhabditis elegans* using a modified Mos1 transposon. *Nat. Methods* **11**, 529-534. doi:10.1038/nmeth.2889
- Gebala, V., Collins, R., Geudens, I., Phng, L.-K. and Gerhardt, H. (2016). Blood flow drives lumen formation by inverse membrane blebbing during angiogenesis *in vivo*. *Nat. Cell Biol.* **18**, 443-450. doi:10.1038/ncb3320
- Gururaja Rao, S., Ponnalagu, D., Sukur, S., Singh, H., Sanghvi, S., Mei, Y., Jin, D. J. and Singh, H. (2017). Identification and characterization of a bacterial homolog of chloride intracellular channel (CLIC) protein. *Sci. Rep.* **7**, 8500. doi:10.1038/s41598-017-08742-z
- Harrop, S. J., Demaere, M. Z., Fairlie, W. D., Reztsova, T., Valenzuela, S. M., Mazzanti, M., Tonini, R., Qiu, M. R., Jankova, L., Warton, K. et al. (2001). Crystal structure of a soluble form of the intracellular chloride ion channel CLIC1 (NCC27) at 1.4-Å resolution. *J. Biol. Chem.* **276**, 44993-45000. doi:10.1074/jbc.M107804200
- Hiley, E., McMullan, R. and Nurrish, S. J. (2006). The G α 12-RGS RhoGEF-RhoA signalling pathway regulates neurotransmitter release in *C. elegans*. *EMBO J.* **25**, 5884-5895. doi:10.1038/sj.emboj.7601458
- Hsieh, J., Liu, J., Kostas, S. A., Chang, C., Sternberg, P. W. and Fire, A. (1999). The RING finger/B-box factor TAM-1 and a retinoblastoma-like protein LIN-35 modulate context-dependent gene silencing in *Caenorhabditis elegans*. *Genes Dev.* **13**, 2958-2970. doi:10.1101/gad.13.22.2958
- Iruela-Arispe, M. L. and Beitel, G. J. (2013). Tubulogenesis. *Development* **140**, 2851-2855. doi:10.1242/dev.070680
- Jansen, G., Thijssen, K. L., Werner, P., Van Der Horst, M., Hazendonk, E. and Plasterk, R. H. A. (1999). The complete family of genes encoding G proteins of *Caenorhabditis elegans*. *Nat. Genet.* **21**, 414-419. doi:10.1038/7753
- Kamei, M., Saunders, W. B., Bayless, K. J., Dye, L., Davis, G. E. and Weinstein, B. M. (2006). Endothelial tubes assemble from intracellular vacuoles *in vivo*. *Nature* **442**, 453-456. doi:10.1038/nature04923
- Kim, W., Underwood, R. S., Greenwald, I. and Shaye, D. D. (2018). OrthoList 2: a new comparative genomic analysis of human and *Caenorhabditis elegans* genes. *Genetics* **210**, 445-461. doi:10.1534/genetics.118.301307
- Kishore, R. S. and Sundaram, M. V. (2002). *ced-10* Rac and *mig-2* function redundantly and act with *unc-73* trio to control the orientation of vulval cell divisions and migrations in *Caenorhabditis elegans*. *Dev. Biol.* **241**, 339-348. doi:10.1006/dbio.2001.0513
- Kjølner, L. and Hall, A. (1999). Signaling to Rho GTPases. *Exp. Cell Res.* **253**, 166-179. doi:10.1006/excr.1999.4674
- Korswagen, H. C., Park, J. H., Ohshima, Y. and Plasterk, R. H. (1997). An activating mutation in a *Caenorhabditis elegans* Gs protein induces neural degeneration. *Genes Dev.* **11**, 1493-1503. doi:10.1101/gad.11.12.1493
- Lai, J.-G., Tsai, S.-M., Tu, H.-C., Chen, W.-C., Kou, F.-J., Lu, J.-W., Wang, H.-D., Huang, C.-L. and Yuh, C.-H. (2014). Zebrafish WNK lysine deficient protein kinase 1 (*wnk1*) affects angiogenesis associated with VEGF signaling. *PLoS ONE* **9**, e106129. doi:10.1371/journal.pone.0106129
- Lant, B., Yu, B., Goudreaux, M., Holmyard, D., Knight, J. D. R., Xu, P., Zhao, L., Chin, K., Wallace, E., Zhen, M. et al. (2015). CCM-3/STRIPAK promotes seamless tube extension through endocytic recycling. *Nat. Commun.* **6**, 6449. doi:10.1038/ncomms7449
- Lecat, S., Matthes, H. W. D., Pepperkok, R., Simpson, J. C. and Galzi, J.-L. (2015). A fluorescent live imaging screening assay based on translocation criteria identifies novel cytoplasmic proteins implicated in G protein-coupled receptor signaling pathways. *Mol. Cell. Proteomics* **14**, 1385-1399. doi:10.1074/mcp.M114.046698
- Li, Y., Shen, X.-X., Evans, B., Dunn, C. W. and Rokas, A. (2021). Rooting the animal tree of life. *Mol. Biol. Evol.* **38**, 4322-4333. doi:10.1093/molbev/msab170
- Liang, J., Shaulov, Y., Savage-Dunn, C., Boissinot, S. and Hoque, T. (2017). Chloride intracellular channel proteins respond to heat stress in *Caenorhabditis elegans*. *PLoS ONE* **12**, e0184308. doi:10.1371/journal.pone.0184308
- Littler, D. R., Harrop, S. J., Brown, L. J., Pankhurst, G. J., Mynott, A. V., Luciani, P., Mandyam, R. A., Mazzanti, M., Tanda, S., Berryman, M. A. et al. (2008). Comparison of vertebrate and invertebrate CLIC proteins: the crystal

- structures of *Caenorhabditis elegans* EXC-4 and *Drosophila melanogaster* DmCLIC. *Proteins* **71**, 364–378. doi:10.1002/prot.21704
- Littlewood, D. T. J. (2017). Animal evolution: last word on sponges-first? *Curr. Biol.* **27**, R259–R261. doi:10.1016/j.cub.2017.02.042
- Lundquist, E. A., Reddien, P. W., Hartwig, E., Horvitz, H. R. and Bargmann, C. I. (2001). Three *C. elegans* Rac proteins and several alternative Rac regulators control axon guidance, cell migration and apoptotic cell phagocytosis. *Development* **128**, 4475–4488. doi:10.1242/dev.128.22.4475
- Ma, X. X., Jiang, Y. L., He, Y. X., Bao, R., Chen, Y. and Zhou, C. Z. (2009). Structures of yeast glutathione-S-transferase Glt2 reveal a new catalytic type of GST family. *EMBO Rep.* **10**, 1320–1326. doi:10.1038/embor.2009.216
- Maduro, M. and Pilgrim, D. (1996). Conservation of function and expression of *unc-119* from two *Caenorhabditis* species despite divergence of non-coding DNA. *Gene* **183**, 77–85. doi:10.1016/S0378-1119(96)00491-X
- Mao, D. Y., Kleinjan, M. L., Jilishitz, I., Swaminathan, B., Obinata, H., Komarova, Y. A., Bayless, K. J., Hla, T. and Kitajewski, J. K. (2021). CLIC1 and CLIC4 mediate endothelial S1P receptor signaling to facilitate Rac1 and RhoA activity and function. *Sci. Signal.* **14**, eabc0425. doi:10.1126/scisignal.abc0425
- Marcus-Gueret, N., Schmidt, K. L. and Stringham, E. G. (2012). Distinct cell guidance pathways controlled by the Rac and Rho GEF domains of UNC-73/TRIO in *Caenorhabditis elegans*. *Genetics* **190**, 129–142. doi:10.1534/genetics.111.134429
- Miller, D. M., III and Niemeyer, C. J. (1995). Expression of the *unc-4* homeoprotein in *Caenorhabditis elegans* motor neurons specifies presynaptic input. *Development* **121**, 2877–2886. doi:10.1242/dev.121.9.2877
- Mosaddeghzadeh, N. and Ahmadian, M. R. (2021). The RHO family GTPases: mechanisms of regulation and signaling. *Cells* **10**, 1831. doi:10.3390/cells10071831
- Nance, J. and Frøkjær-Jensen, C. (2019). The *Caenorhabditis elegans* transgenic toolbox. *Genetics* **212**, 959–990. doi:10.1534/genetics.119.301506
- Noma, K. and Jin, Y. (2016). Optogenetic random mutagenesis using histone-miniSOG in *C. elegans*. *J. Vis. Exp.*, **117**, e54810. doi:10.3791/54810
- Nørgaard, S., Deng, S., Cao, W. and Pocock, R. (2018). Distinct CED-10/Rac1 domains confer context-specific functions in development. *PLoS Genet.* **14**, e1007670. doi:10.1371/journal.pgen.1007670
- Peters, E. C., Gossett, A. J., Goldstein, B., Der, C. J. and Reiner, D. J. (2013). Redundant canonical and noncanonical *Caenorhabditis elegans* p21-activated kinase signaling governs distal tip cell migrations. *G3 (Bethesda)* **3**, 181–195. doi:10.1534/g3.112.004416
- Ponsioen, B., Van Zeijl, L., Langeslag, M., Berryman, M., Littler, D., Jalink, K. and Moolenaar, W. H. (2009). Spatiotemporal regulation of chloride intracellular channel protein CLIC4 by RhoA. *Mol. Biol. Cell* **20**, 4664–4672. doi:10.1091/mbc.e09-06-0529
- Reddien, P. W. and Horvitz, H. R. (2000). CED-2/CrkII and CED-10/Rac control phagocytosis and cell migration in *Caenorhabditis elegans*. *Nat. Cell Biol.* **2**, 131–136. doi:10.1038/35004000
- Redemann, S., Schloissnig, S., Ernst, S., Pozniakowsky, A., Ayloo, S., Hyman, A. A. and Bringmann, H. (2011). Codon adaptation-based control of protein expression in *C. elegans*. *Nat. Methods* **8**, 250–252. doi:10.1038/nmeth.1565
- Reiner, D. J. and Lundquist, E. A. (2018). Small GTPases. *WormBook* **2018**, 1–65. doi:10.1895/wormbook.1.67.2
- Ros-Rocher, N., Pérez-Posada, A., Leger, M. M. and Ruiz-Trillo, I. (2021). The origin of animals: an ancestral reconstruction of the unicellular-to-multicellular transition. *Open Biol.* **11**, 200359. doi:10.1098/rsob.200359
- Schade, M. A., Reynolds, N. K., Dollins, C. M. and Miller, K. G. (2005). Mutations that rescue the paralysis of *Caenorhabditis elegans* ric-8 (synembryo) mutants activate the G α (s) pathway and define a third major branch of the synaptic signaling network. *Genetics* **169**, 631–649. doi:10.1534/genetics.104.032334
- Sehnal, D., Bittrich, S., Deshpande, M., Svobodová, R., Berka, K., Bazgier, V., Velankar, S., Burley, S. K., Koča, J. and Rose, A. S. (2021). Mol* Viewer: modern web app for 3D visualization and analysis of large biomolecular structures. *Nucleic Acids Res.* **49**, W431–W437. doi:10.1093/nar/gkab314
- Shakir, M. A., Gill, J. S. and Lundquist, E. A. (2006). Interactions of UNC-34 Enabled with Rac GTPases and the NIK kinase MIG-15 in *Caenorhabditis elegans* axon pathfinding and neuronal migration. *Genetics* **172**, 893–913. doi:10.1534/genetics.105.046359
- Shakir, M. A., Jiang, K., Struckhoff, E. C., Demarco, R. S., Patel, F. B., Soto, M. C. and Lundquist, E. A. (2008). The Arp2/3 activators WAVE and WASP have distinct genetic interactions with Rac GTPases in *Caenorhabditis elegans* axon guidance. *Genetics* **179**, 1957–1971. doi:10.1534/genetics.108.088963
- Shaye, D. D. and Greenwald, I. (2011). OrthoList: a compendium of *C. elegans* genes with human orthologs. *PLoS ONE* **6**, e20085. doi:10.1371/journal.pone.0020085
- Shaye, D. D. and Greenwald, I. (2015). The disease-associated formin INF2/EXC-6 organizes lumen and cell outgrowth during tubulogenesis by regulating F-actin and microtubule cytoskeletons. *Dev. Cell* **32**, 743–755. doi:10.1016/j.devcel.2015.01.009
- Shaye, D. D. and Greenwald, I. (2016). A network of conserved formins, regulated by the guanine exchange factor EXC-5 and the GTPase CDC-42, modulates tubulogenesis in vivo. *Development* **143**, 4173–4181. doi:10.1242/dev.141861
- Shaye, D. D. and Soto, M. C. (2021). Epithelial morphogenesis, tubulogenesis and forces in organogenesis. *Curr. Top. Dev. Biol.* **144**, 161–214. doi:10.1016/bs.ctdb.2020.12.012
- Struckhoff, E. C. and Lundquist, E. A. (2003). The actin-binding protein UNC-115 is an effector of Rac signaling during axon pathfinding in *C. elegans*. *Development* **130**, 693–704. doi:10.1242/dev.00300
- Sundaram, M. V. and Buechner, M. (2016). The *Caenorhabditis elegans* excretory system: a model for tubulogenesis, cell fate specification, and plasticity. *Genetics* **203**, 35–63. doi:10.1534/genetics.116.189357
- Syrovatkin, V., Alegre, K. O., Dey, R. and Huang, X.-Y. (2016). Regulation, signaling, and physiological functions of G-proteins. *J. Mol. Biol.* **428**, 3850–3868. doi:10.1016/j.jmb.2016.08.002
- Tavasoli, M., Al-Momany, A., Wang, X., Li, L., Edwards, J. C. and Ballermann, B. J. (2016a). Both CLIC4 and CLIC5A activate ERM proteins in glomerular endothelium. *Am. J. Physiol. Renal. Physiol.* **311**, F945–F957. doi:10.1152/ajprenal.00353.2016
- Tavasoli, M., Li, L., Al-Momany, A., Zhu, L.-F., Adam, B. A., Wang, Z. and Ballermann, B. J. (2016b). The chloride intracellular channel 5A stimulates podocyte Rac1, protecting against hypertension-induced glomerular injury. *Kidney Int.* **89**, 833–847. doi:10.1016/j.kint.2016.01.001
- Thompson, J. D., Higgins, D. G. and Gibson, T. J. (1994). CLUSTAL W: improving the sensitivity of progressive multiple sequence alignment through sequence weighting, position-specific gap penalties and weight matrix choice. *Nucleic Acids Res.* **22**, 4673–4680. doi:10.1093/nar/22.22.4673
- Thompson, O., Edgley, M., Strasbourger, P., Flibotte, S., Ewing, B., Adair, R., Au, V., Chaudhry, I., Fernando, L., Hutter, H. et al. (2013). The million mutation project: a new approach to genetics in *Caenorhabditis elegans*. *Genome Res.* **23**, 1749–1762. doi:10.1101/gr.157651.113
- Tung, J. J. and Kitajewski, J. (2010). Chloride intracellular channel 1 functions in endothelial cell growth and migration. *J. Angiogenesis Res.* **2**, 23. doi:10.1186/2040-2384-2-23
- Tung, J. J., Hobert, O., Berryman, M. and Kitajewski, J. (2009). Chloride intracellular channel 4 is involved in endothelial proliferation and morphogenesis in vitro. *Angiogenesis* **12**, 209–220. doi:10.1007/s10456-009-9139-3
- Ulasov, B., Bruno, J., Gordon, N., Hartnett, M. E. and Edwards, J. C. (2009). Chloride intracellular channel protein-4 functions in angiogenesis by supporting acidification of vacuoles along the intracellular tubulogenic pathway. *Am. J. Pathol.* **174**, 1084–1096. doi:10.2353/ajpath.2009.080625
- Van Der Linden, A. M., Moorman, C., Cuppen, E., Korswagen, H. C. and Plasterk, R. H. A. (2003). Hyperactivation of the G12-mediated signaling pathway in *Caenorhabditis elegans* induces a developmental growth arrest via protein kinase C. *Curr. Biol.* **13**, 516–521. doi:10.1016/S0960-9822(03)00164-7
- Vidal, B., Aghayeva, U., Sun, H., Wang, C., Glenwinkel, L., Bayer, E. A. and Hobert, O. (2018). An atlas of *Caenorhabditis elegans* chemoreceptor expression. *PLoS Biol.* **16**, e2004218. doi:10.1371/journal.pbio.2004218
- Xie, J., Wu, T., Xu, K., Huang, I. K., Cleaver, O. and Huang, C.-L. (2009). Endothelial-specific expression of WNK1 kinase is essential for angiogenesis and heart development in mice. *Am. J. Pathol.* **175**, 1315–1327. doi:10.2353/ajpath.2009.090094
- Xie, J., Yoon, J., Yang, S.-S., Lin, S.-H. and Huang, C.-L. (2013). WNK1 protein kinase regulates embryonic cardiovascular development through the OSR1 signaling cascade. *J. Biol. Chem.* **288**, 8566–8574. doi:10.1074/jbc.M113.451575
- Xu, K. and Cleaver, O. (2011). Tubulogenesis during blood vessel formation. *Semin. Cell Dev. Biol.* **22**, 993–1004. doi:10.1016/j.semcdb.2011.05.001
- Yu, J. A., Castranova, D., Pham, V. N. and Weinstein, B. M. (2015). Single-cell analysis of endothelial morphogenesis in vivo. *Development* **142**, 2951–2961. doi:10.1242/dev.123174
- Zhuravlev, Y., Hirsch, S. M., Jordan, S. N., Dumont, J., Shirasu-Hiza, M. and Canman, J. C. (2017). CYK-4 regulates Rac, but not Rho, during cytokinesis. *Mol. Biol. Cell* **28**, 1258–1270. doi:10.1091/mbc.e17-01-0020
- Zipkin, I. D., Kindt, R. M. and Kenyon, C. J. (1997). Role of a new Rho family member in cell migration and axon guidance in *C. elegans*. *Cell* **90**, 883–894. doi:10.1016/S0092-8674(00)80353-0